How reliable are CMIP5 models in simulating dust optical depth?

Bing Pu[1,2] and Paul Ginoux[2]

[1]Atmospheric and Oceanic Sciences Program, Princeton University,

Princeton, New Jersey 08544

[2]NOAA Geophysical Fluid Dynamics Laboratory, Princeton, New Jersey 08540

Correspondence to: Bing Pu (bpu@princeton.edu)

Abstract. Dust aerosol plays an important role in the climate system by affecting the radiative and energy balances. Biases in dust modeling may result in biases in simulating global energy budget and regional climate. It is thus very important to understand how well dust is simulated in the Coupled Model Intercomparison Project Phase 5 (CMIP5) models. Here seven CMIP5 models using interactive dust emission schemes are examined against satellite derived dust optical depth (DOD) during 2004-2016.

It is found that multi-model mean can largely capture the global spatial pattern and zonal mean of DOD over land in present-day climatology in MAM and JJA. Global mean land DOD is underestimated by -25.2% in MAM to -6.4% in DJF. While seasonal cycle, magnitude, and spatial pattern are generally captured by multi-model mean over major dust source regions such as North Africa and the Middle East, these variables are not so well represented by most of the models in South Africa and Australia. Interannual variations of DOD are neither captured by most of the models nor by multi-model mean. Models also do not capture the observed connections between DOD and local controlling factors such as surface wind speed, bareness, and precipitation. The constraints from surface bareness are largely underestimated while the influences of surface wind and precipitation are overestimated.

Projections of DOD change in the late half of the 21st century under the Representative Concentration Pathways 8.5 scenario by multi-model mean is compared with those projected by a regression model. Despite the uncertainties associated with both projections, results show some similarities between the two, e.g., DOD pattern over North Africa in DJF and JJA, an increase of DOD in the central Arabian Peninsula in all seasons, and a decrease over northern China from MAM to SON.

1. Introduction

Dust is the second most abundant aerosols by mass in the atmosphere after sea salt. It absorbs and scatters both shortwave and longwave radiation and thus modifies local radiative budget and consequently vertical temperature profile, influencing global and regional climate. For instance, studies found dust influences the strength of the West African monsoon (e.g., Miller and Tegen, 1998; Miller et al., 2004; Mahowald et al., 2010; Strong et al., 2015) and Indian monsoonal rainfall (e.g., Vinoj et al., 2014; Jin et al., 2014, 2015, 2016; Solmon et al., 2015; Kim et al., 2016; Sharma and Miller, 2017). Dust aerosols are also found to amplify droughts during the U.S. Dust Bowl and Medieval Climate Anomaly (Cook et al., 2008, 2009, 2013), and affect Atlantic tropical cyclones (e.g., Dunion and Velden, 2004; Wong and Dessler, 2005; Evan et al., 2006; Sun et al., 2008; Strong et al., 2018). Dust particles can also serve as ice cloud nuclei and influence the properties of the cloud (e.g., Levin et al., 1996; Rosenfield et al., 1997; Wurzler et al., 2000; Nakajima et al., 2001; Bangert et al., 2012) and affect regional radiative balance and hydrological cycle. When deposited in the oceans, iron-enriched dust also provides nutrients for phytoplankton, affecting ocean productivity and therefore carbon and nitrogen cycles and ocean albedo (e.g., Fung et al., 2000; Jickells et al., 2005; Shao et al., 2011).

Globally, the estimated radiative forcing from dust aerosol is 0.10 (-0.30 to +0.10) W m^{-2}, a magnitude about one fourth of the radiative forcing of sulfate aerosol or black carbon from fossil fuel and biofuel (Myhre et al., 2013; their Table 8.4). Biases in dust simulation may potentially affect global energy budgets and regional climate simulation.

Thus, it is very important to examine the capability of current state-of-the-art climate models in simulating dust.

Only a few studies examined the Coupled Model Intercomparison Project Phase 5 (CMIP5) model output of dust and most of them are regional evaluations. For instance, Evan et al. (2014) examined model output for Africa, but mainly focused on an area over the northeastern Atlantic (10°–20°N and 20°–30°W) where a long-term proxy of dust optical depth data over Cape Verde islands is available (Evan and Mukhopadhyay, 2010). They found models underestimated dust emission and mass path and failed to capture the interannual variations from 1960 to 2004, as models did not capture the negative connection between dust mass path and precipitation over the Sahel.

Another work examined CMIP5 aerosol optical depth (AOD) is by Sanap et al. (2014) for India. They compared dust distribution in the models with Earth Probe total ozone monitoring system (EPTOMS)/ Ozone monitoring Instrument (OMI) aerosol index (AI) from 2000 to 2005. They found most of CMIP5 models, except two HadGEM2 models, underestimated dust load over Indo-Gangetic Plains, and suggested the biases are due to a misrepresentation of 850 hPa winds in the models. Later, Misra et al. (2016) also examined CMIP5 modeled AOD for India but did not specifically focus on dust.

Shindell et al. (2013) examined the output of 10 models from the Atmospheric Chemistry and Climate Model Intercomparison Project (ACCMIP) for one year (2000), among which eight models also participated in the CMIP5. They noticed that simulated dust AOD vary by more than a factor of two across models. However, this study also did not focus on dust, but emphasized the radiative forcings from anthropogenic aerosols.

None of the above studies examined global dust simulation in CMIP5 models. What's more, most studies focused on annual mean, not seasonal averages. It is very possible that models perform better in some seasons than others. AeroCom multiple-dust model intercomparison was performed on both global and regional scales (Huneeus et al., 2011) but only focused on one year, thus models' capability of simulating interannual or long-term variability of dust is not clear. A comprehensive evaluation of the climatology and interannual variation of global dust optical depth (DOD) in CMIP5 models will provide insights into models' capability of simulating the integrated aerosol extinction due to dust, which is one of the key variables that determine the radative forcing of dust to the climate system.

Here we examine the results of seven CMIP5 models (Table 1) by comparing model output with DOD derived from Moderate Resolution Imaging Spectroradiometer (MODIS) Deep Blue aerosol products. Projections on changes of DOD in the late half of the 21st century by CMIP5 models and also by a regression model (Pu and Ginoux, 2017) are examined and analyzed. The following section introduces data and methods used in this study. Results are presented in section 3, including examinations on the climatology and interannual variations of CMIP5 DOD and future projections. Discussion and major conclusions are presented in sections 4 and 5, respectively.

2. Data and Methodology

2.1 DOD from MODIS

DOD is a widely used variable that describes optical depth due to the extinction by mineral particles. It is one of the key factors (single scattering albedo and asymmetry

91 factor being the two others) controlling dust interaction with radiation. Monthly DOD are
92 derived from MODIS aerosol products retrieved using the Deep Blue (MDB2) algorithm,
93 which employs radiance from the blue channels to detect aerosols globally over land even
94 over bright surfaces, such as desert (Hsu et al., 2004, 2006). Ginoux et al. (2012b) used
95 collection 5.1 level 2 aerosol products from MODIS aboard the Aqua satellite to derive
96 DOD. Here, both MODIS aerosol products (collection 6, level 2; Hsu et al., 2013) from
97 the Aqua and Terra platforms are used. Aerosol products such as AOD (550 nm), single
98 scattering albedo, and the Ångström exponent are first interpolated to a regular 0.1° by
99 0.1° grid using the algorithm described by Ginoux et al. (2010). The DOD is then derived
100 from AOD following the methods of Ginoux et al. (2012b) with adaptions for the newly
101 released MODIS collection 6 aerosol products (Pu and Ginoux, 2016). To separate dust
102 from other aerosols, we use the Ångström exponent (α) and single scattering albedo (ω).
103 Ångström exponent has been shown to be highly sensitive to particle size (Eck et al.,
104 1999). A continuous function relating the Ångström exponent to fine-mode aerosol
105 optical depth established by Anderson et al. (2005; their Eq. 5) based on ground-based
106 data is used to separate dust from fine particles. We also screen the data by setting single
107 scattering albedo at 470 nm to be less than one for dust due to its absorption of solar
108 radiation. This separates dust from scattering aerosols such as sea salt, which is purely
109 scattering. The formula can be summarized as the following:

110 $$DOD = AOD \times (0.98\text{-}0.5089\alpha + 0.0512\alpha^2) \quad \text{if } (\omega < 1) \quad . \qquad (1)$$
111

112 Note that DOD represents the coarse mode fraction of dust only. It is estimated that the
113 fine mode dust at emission is less than 10% (Kok et al., 2017).

Aqua and Terra DOD have previously been used to study global dust sources (Ginoux et al., 2012b), and their geomorphological signature (Baddock et al., 2016), dust variations in the Middle East (Pu and Ginoux, 2016) and the U.S. (Pu and Ginoux, 2017), and have been validated with Aerosol Robotic NETwork (AERONET) stations over the U.S. (Pu and Ginoux, 2017). Here we compare Aqua and Terra DOD against AERONET stations globally (Section 1 and Figures. S1-2 in the Supplement). Both Aqua and Terra DOD is slightly underestimated, with respective errors of 0.08+0.52DOD and 0.10+0.48DOD.

Daily DOD from Aqua and Terra are averaged to monthly data and interpolated to a 1° by 1° grid. Terra passes the Equator from north to south around 10:30 local time while Aqua passes the Equator from south to north around 13:30 local time. To reduce missing data and also to combine the information from both morning and afternoon hours, a combined monthly DOD (here after MODIS DOD) is derived by averaging Aqua and Terra DOD when both products exist or using either Aqua or Terra DOD when only one product is available. As shown in Figure S3 in the Supplement, the mean available days in each season and also spatial coverage are enhanced in combined DOD than using Aqua or Terra (not shown) DOD alone. This combined DOD is available from January 2003 to December 2016.

We also compared MODIS DOD climatology with both AERONET observation and DOD retrieved from Cloud-Aerosol Lidar with Orthogonal Polarization (CALIOP; Winker et al., 2004; 2007) aboard the Cloud-Aerosol Lidar and Infrared Pathfinder Satellite Observation (CALIPSO) satellite. AERONET stations provide cloud-screened and quality assured (level 2) coarse mode aerosol optical depth (COD) at 500 nm, which

137 is processed by the Spectral Deconvolution Algorithm (O'Neill et al., 2003). Only nine
138 sites have long-term COD records during 2003-2016, and the climatological mean of
139 MODIS DOD generally compares well with these sites (Figure S4 in the Supplement).

140 CALIOP measures backscattered radiances attenuated by the presence of aerosols
141 and clouds and retrieves corresponding microphysical and optical properties of aerosols.
142 Monthly dust AOD (or DOD) on a 2° latitude by 5° longitude grid are available since
143 June 2006. The climatology of CALIOP DOD during 2007-2016 is similar to that of
144 MODIS DOD during the same period (Figure S5 in the Supplement). The global mean
145 (over land) MODIS DOD is slightly higher than that from CALIOP, probably due to the
146 lower horizontal resolution of the latter. The pattern correlations (e.g., Pu et al., 2016)
147 between the two products range from 0.83 in boreal spring and summer to 0.63 in boreal
148 winter (Figure S5 in the Supplement). Due to higher spatial resolution (compared with
149 CALIOP) and coverage (compared with AERONET sites), MODIS DOD is chosen as the
150 primary product to validate CMIP5 model output. Nine regions (Table 2) are selected to
151 study the DOD magnitude, spatial pattern, and variations. These regions cover major dust
152 source regions previously identified (Ginoux et al. 2012).

153 Given the analysis above (Figs. S3-5), there are some uncertainties associated
154 with DOD in a few regions in some seasons: (1) relatively low coverage (<30 days per
155 season) over northern China and southeastern Asia in JJA; (2) DOD is slightly higher
156 than COD from AERONET over the Arabian Peninsula in DJF and SON; (3) DOD is
157 lower than CALIOP over northern India in MAM. We will consider these uncertainties in
158 the following analysis wherever is relevant.
159

2.2 Reanalysis and observation datasets

Previous study found that the variations of dust event frequency over the U.S. in the recent decade could be largely represented by the variations of three local controlling factors: seasonal mean surface wind speed, bareness, and precipitation (Pu and Ginoux, 2017). These factors have previously been found to constrain dust emission or variability on multiple time scales (e.g., Gillette and Passi, 1988; Fecan et al., 1999; Zender and Kwon, 2005). While surface wind is positively related to the emission and transport of dust, vegetation is an important non-erodible element that prevents wind erosion. Precipitation is generally negatively related to dust emission and transport processes. While the scavenging effect of precipitation on small dust particles only lasts a few hours or days, influences of precipitation on soil moisture lasts longer.

To examine the interannual variations of DOD and its connection with local controlling factors such as surface wind speed, bareness, and precipitation, monthly data of 10 m wind speed from the ERA-Interim (Dee et al., 2011), leaf area index (LAI) data from Advanced Very High Resolution Radiometer (AVHRR; Claverie et al., 2014, 2016), and precipitation from the Precipitation Reconstruction over Land (PRECL; Chen et al., 2002) are used.

ERA-Interim is a global reanalysis from the European Centre for Medium-Range Weather Forecasts (ECMWF). Its horizontal resolution is T255 (about 0.75° or 80 km). We choose this analysis because of its relatively high spatial resolution. The monthly data are available from 1979 to present day.

Monthly LAI derived from the version 4 of Climate Data Record (CDR) of AVHRR is used to calculate surface bareness. The data are produced by the National

183 Aeronautics and Space Administration (NASA) Goddard Space Flight Center (GSFC)
184 and the University of Maryland. Monthly gridded data on a horizontal resolution of 0.05°
185 by 0.05° degree are available from 1981 to present. This product is selected due to its
186 high spatial resolution and long temporal coverage. Surface bareness is calculated from
187 seasonal mean LAI (Pu and Ginoux, 2017) as the following,

188 $$Bareness = exp\ (-LAI) \quad . \quad (2)$$

189 Bareness is originally defined as *exp (-LAI-SAI)*, where *SAI* is stem area index (Evans et
190 al. 2016). Since satellite does not retrieve brownish SAI, we only use LAI to calculate
191 bareness.

192 PRECL precipitation from the National Oceanic and Atmospheric Administration
193 (NOAA) is a global analysis available monthly from 1948 to present at a 1° by 1°
194 resolution. The dataset is derived from gauge observations from the Global Historical
195 Climatology Network (GHCN), version 2, and the Climate Anomaly Monitoring System
196 (CAMS) datasets. Its long coverage and spatial resolution is suitable to study the
197 connections between DOD and precipitation.

198

199 **2.3 CMIP5 model output**

200 Among CMIP5 models we selected seven models (Table 1) that used interactive
201 dust emission schemes, in which dust emission varied in response to changes of climate.
202 The output of 10 m wind speed, precipitation, and LAI are also available from these
203 models. In models that dust is simulated offline, i.e., dust emission did not interactively
204 respond to meteorological and climate changes, the connections between DOD and
205 modeled controlling factors are lost. Other models (to our best knowledge) either used

offline dust as an input or did not write out the variables needed for this analysis.

Both historical run from 1861 to 2005 and future run under the Representative Concentration Pathways 8.5 (RCP 8.5) scenario (Riahi et al., 2011) from 2006 to 2100 are used. Here the RCP 8.5 scenario is chosen because it represents the upper limit of the projected greenhouse gas change in the twenty-first century and thus likely is the worst-case scenario for future DOD variation under climate change. Also, studies found that observed CO_2 emission pathway during 2005-2014 matches RCP 8.5 scenario better than other scenarios (e.g., Fuss et al., 2014), which makes the RCP8.5 output suitable to examine present-day DOD variations after 2005.

Monthly model output of dust load, surface 10 m wind speed, precipitation, and LAI are used. Historical output from 2003 to 2005 and RCP 8.5 output from 2006 to 2016 are combined to form time series and climatology during 2003-2016 to compare with MODIS DOD during the same time period.

2.3.1 DOD derived from modeled dust load

Most CMIP5 models did not save DOD, so we used monthly dust load and converted them to DOD using the relationship derived by Ginoux et al. (2012a) as the following

$$\tau = M \times e \ , \quad (3)$$

where τ is DOD at 500 nm, M is the load of dust in unit of (g m^{-2}), and e = 0.6 m^2 g^{-1} is the mass extinction efficiency. Dust load from different models is first interpolated to a 2° by 2.5° grid and then converted to DOD. The same method was used by Pu and Ginoux (2017) for the U.S. Applying the same mass extinction efficiency everywhere

and to all the CMIP5 model output used here is a simplification, as different models may have quite different mass extinction efficiency. For instance, e can range from 0.25 to 1.28 $m^2 g^{-1}$ in AEROCOM models, with a multi-model medium of 0.72 $m^2 g^{-1}$ (Huneeus et al., 2011). Here, we compare the derived DOD with modeled DOD from one historical simulation of GFDL-CM3 model (Donner et al., 2011) as an example. A full validation of this method will require modeled DOD from all the other CMIP5 models, which are currently not available. The pattern correlation of the climatology (1861-2005) between the derived DOD and modeled DOD in GFDL-CM3 are very high, all above 0.99 for four seasons (not shown). The percentage differences between derived DOD and modeled DOD averaged over global land range from -3.6% in DJF and SON to 1.3% in MAM and JJA.

2.4 A linear regression model

2.4.1 Multiple linear regression

In order to examine the relative contribution of each local controlling factor to DOD variations, multiple linear regression is applied by regressing MODIS DOD onto standardized seasonal mean ERA-Interim surface wind speed, AVHRR bareness, and PRECL precipitation at each grid point. All the data are re-gridded to a 1° by 1° grid before the calculation. Over regions where values are missing for any of the explanatory variables (i.e., precipitation, bareness, and surface wind speed) or DOD, the regression coefficients are set to missing values. The collinearity among these explanatory variables is examined by calculating variance inflation factor (VIF) (e.g., O'Brien, 2007; Abudu et al., 2011), and in most regions the VIF is below 2 (not shown), indicating a low

252 collinearity (5–10 is usually considered high). Bootstrap resampling is used to test the
253 significance of the regression coefficients, following the method used by Pu and Ginoux
254 (2017).

255 Multiple linear regression is also applied to CMIP5 model derived DOD and
256 output of surface wind speed, bareness, and precipitation to obtain regression coefficients
257 from the models from 2004 to 2016. All variables are interpolated to a 2° by 2.5° grid
258 before regression. The results are compared with regression coefficients derived from
259 observational datasets.

260

261 **2.4.2 DOD reconstruction and future projection**

262 Using regression coefficients obtained from observations and observed variations
263 of precipitation, bareness, and surface wind speed from 2004 to 2016, we can reconstruct
264 DOD in the present day and compare it with MODIS DOD (see discussion in section 3.2).

265 Similar to the method used by Pu and Ginoux (2017), the regression coefficients
266 derived from MODIS DOD and observed controlling factors and CMIP5 model output of
267 surface wind speed, bareness, and precipitation are used to project variations of future
268 DOD. The regression coefficients are interpolated from the 1° by 1° grid to a 2° by 2.5°
269 grid to be consistent with model output. Such an interpolation may smooth out some
270 spatial characteristics from observations. Here we tried two groups of CMIP5 output for
271 these controlling factors. One group used seven models with interactive dust emission
272 scheme (Table 1), and the other used 16 CMIP5 models (see Supplementary Table S1 of
273 Pu and Ginoux, 2017) that include the seven models with interactive dust emission
274 scheme. The reason to test the latter is to include as much model output of the controlling

275 factors as possible. The differences between the historical run (1861–2005 average) and
276 that of the RCP 8.5 run for the late half of the twenty-first century (2051–2100) are
277 standardized by the standard deviation of the historical run for each explanatory variable.
278 The projected change reveals how DOD will vary with reference to the historical
279 conditions (mean and standard deviation).
280
281 **3. Results**
282 **3.1 Climatology (2004-2016)**
283 Figure 1 shows the climatology of MODIS DOD (top panel) in four seasons
284 during 2004-2016 and that from the CMIP5 multi-model mean (bottom). Globally, the
285 dustiest regions are largely located over the northern hemisphere (NH) over North Africa,
286 the Middle East, and East Asia (Figs. 1a-d). In these regions, DOD is higher in boreal
287 spring and summer than fall and winter. Modeled global DOD over land is generally
288 lower than that from MODIS DOD, ranging from -0.028 (-25.2%) in MAM to -0.005 (-
289 6.4%) in DJF. The global spatial pattern is better captured in MAM and JJA, with pattern
290 correlations of 0.74 and 0.85, respectively (Figs. 1f-g). In DJF, DOD is overestimated
291 over central Africa and Australia, but underestimated over the Middle East and Asia (Fig.
292 1e), while in SON there is a similar overestimation in Australia and an underestimation in
293 the Middle East (Fig. 1h).
294 Figure 2 shows the zonal mean of CMIP5 DOD from individual models (thin
295 colorful lines) and multi-model ensemble mean (thick black), in comparison with MODIS
296 DOD (thick red). In DJF, DOD is underestimated in the NH from 15° N to 50°N but
297 overestimated over the tropics and southern hemisphere (SH) (Fig. 2a). While the

298 overestimation in the SH is largely contributed by three models, the underestimation in
299 the NH appears in all the seven models. The overestimation of DOD in HadGEM2-ES
300 has also been identified in a previous study (Bellouin et al., 2011) and will be discussed
301 later. In MAM, a similar overestimation of DOD in the tropics and SH also occurs in
302 some models, and the multi-model mean slightly overestimates DOD around 20°-30°S
303 (Fig. 2b). In NH, there is a weak underestimation too, but the overall gradient is largely
304 captured. In JJA, the multi-model mean resembles MODIS DOD very well (Fig. 2c),
305 consistent with the highest pattern correlation in this season shown in Fig. 1. The peak
306 around 19° N in North Africa and Middle East is well captured by the multi-model mean,
307 although the magnitude is slightly underestimated. In SON, different from MODIS DOD
308 that peaks around 19°N, the multi-model mean has two peaks around 15°N and 28°S,
309 respectively, a pattern somewhat similar to that in DJF (Fig. 2d). Consequently, DOD in
310 CMIP5 multi-model mean is overestimated at 15°-40°S and 0°-15°N but underestimated
311 at 15°S -0° and 15°-40°N.

312 Seasonal cycles of CMIP5 DOD are compared with MODIS DOD in nine regions
313 in Figure 3. The annual means of DOD in each region from multi-model mean (black)
314 and MODIS (red) are also listed in each plot. The spread of DOD among individual
315 models is greater during boreal spring and summer for regions in the NH and during
316 austral spring and summer for regions in the SH. Seasonal cycles over North Africa, the
317 Middle East, North America, and India are generally captured by multi-model mean, with
318 modeled DOD peaking during the same seasons as MODIS DOD (Figs. 3a-b, d-e). While
319 some models overestimate the seasonal peaks over the Middle East, North America, and
320 India (e.g., CanESM2, HadGEM2-ES, and HadGEM2-CC), a few models have very

321 weak seasonal cycles and underestimate DOD over North America and India (e.g.,
322 GFDL-CM3, NorESM1-M, MIROC-ESM, and MIROC-ESM-CHEM). Note that
323 MODIS DOD is slightly lower than CALIOP DOD over India in MAM (Fig. S5),
324 therefore for these models the underestimation may be larger than shown in Fig. 3e.

325 Since the temporal coverage of MODIS DOD over northern China and
326 southeastern Asia is relatively low in JJA compared with other regions (Fig. S3), we also
327 examined the seasonal cycle of CALIOP DOD (not shown) and results are similar but
328 with weaker magnitude. Over northern China, MODIS DOD peaks in spring (Fig. 3c),
329 consistent with previous studies (e.g., Zhao et al., 2006; Laurent et al., 2006; Ginoux et
330 al., 2012b), while multi-model mean peaks later in May-June. Individual models have
331 quite different seasonal cycles, with GFDL-CM3 model having a peak (in April) closer to
332 the timing of MODIS maximum. Similar misrepresentation occurs over the southeastern
333 Asia (Fig. 3f).

334 In South Africa and South America the observed maxima in early austral spring
335 (i.e., September) are also not captured by the multi-model mean (Figs. 3g-h). Note that
336 CanESM2 largely captures the seasonal cycle of DOD over South America, although the
337 magnitude is overestimated (Fig. 3h). In Australia, DOD is largely overestimated and the
338 peak from November to January in MODIS DOD is shifted about one month earlier in
339 the multi-model mean (Fig. 3i). Similar to the finding here, Bellouin et al. (2011) also
340 found that HadGEM2-ES model overestimated DOD over Australia and Thar desert
341 region in northwestern India and suggested that these overestimations were likely due to
342 model's overestimation of bare soil fraction and underestimation of soil moisture. Despite

343 overestimation, the seasonal cycle in HadGEM2-CC model is more similar to MODIS
344 DOD than other models (Fig. 3i).

345 We further examine the magnitudes and spatial patterns of CMIP5 DOD in these
346 regions. Figure 4 shows the ratio of pattern standard deviations (standard deviations of
347 values within the domain) and pattern correlation between CMIP5 DOD and MODIS
348 DOD climatology (2004-2016) in each region for four seasons. While the former reveals
349 the magnitude differences, the latter demonstrates the spatial resemblance.

350 Over North Africa, the Middle East, and India, the ratio of CMIP5 DOD from
351 individual models and multi-model mean versus MODIS DOD are all within ± one
352 order of magnitude (Fig. 4). Most models underestimate DOD in northern China,
353 although the magnitudes are largely within the range of -one order of magnitude to one.
354 Over North America, South Africa, and Australia, some models underestimate the DOD
355 by more than two orders of magnitudes, while over Australia three models overestimate
356 DOD by more than one order of magnitude. In general, magnitudes of multi-model mean
357 are closer to satellite DOD than most individual models and are largely within ± one
358 order of magnitude of MODIS DOD.

359 The spatial patterns are better captured over North Africa and the Middle East
360 than other regions (Fig. 4), with pattern correlations above 0.6 in most models (with
361 highest pattern correlation of 0.92 and 0.83, respectively). Pattern correlations from
362 multi-model mean are also high, reaching 0.87 (0.78) over North Africa and 0.75 (0.73)
363 over the Middle East in JJA (MAM). Nonetheless, some models show negative pattern
364 correlations over North Africa, northern China, North America, southeastern Asia, South

365 Africa, South America, and Australia. Overall, spatial patterns are less well represented
366 in regions over the SH than over the NH in CMIP5 models.

367 In short, in terms of both magnitudes and spatial pattern, DOD climatology is best
368 represented over North Africa and the Middle East among the nine regions. The multi-
369 model mean shows that DOD over North Africa is slightly better simulated than over the
370 Middle East, somewhat similar to the finding of AeroCom multi-model analysis
371 (Huneeus et al. 2011).

372

373 **3.2 Interannual variations**

374 An important aspect of dust activity is its long-term variability, including
375 interannual and decadal variations. Dust emission in North Africa is known to have
376 strong decadal variations (e.g., Prospero and Nees, 1986; Prospero and Lamb, 2003;
377 Mahowald et al., 2010; Evan et al., 2014, 2016), while over Australia, strong interannual
378 variations have been related to El Niño–Southern Oscillation (e.g., Marx et al., 2009;
379 Evans et al., 2016). Due to the short time coverage of high quality satellite products, we
380 focus on interannual variations of DOD from 2004 to 2016.

381 Figure 5 shows the correlations of regional mean time series of DOD between
382 MODIS and CMIP5 models and multi-model mean for each season in nine regions. We
383 also show correlations between the reconstructed DOD (see section 2.4.2 for details) and
384 MODIS DOD for reference (Table S1 in the Supplement). The reconstructed DOD is
385 calculated using observed regression coefficients and time-varying controlling factors
386 from observations (i.e., surface wind speed, bareness, and precipitation).

387 The interannual variations of DOD are in general not well captured by CMIP5
388 models. This is consistent with previous study by Evan et al. (2014) who found dust
389 variability downwind of North Africa over the northeastern Atlantic was misrepresented
390 in CMIP5 models. In most regions, only one or two models show significant positive
391 correlation with MODIS DOD in some seasons, and negative correlations exist in all
392 regions (Fig. 5). North Africa, the Middle East, southeastern Asia, South America, and
393 Australia show less negative correlations than other dusty regions. On the other hand,
394 reconstructed DOD shows significant positive correlations with MODIS DOD over most
395 regions in all seasons (Table S1 in the Supplement). This suggests that the interannual
396 variations of DOD can be largely attributed to the variations of these controlling factors,
397 and models may misrepresent these relationships, in addition to their incapacity of
398 capturing the interannual variations of individual controlling factors in general (not
399 shown), which is not uncommon for coupled models.
400 We further examine the connection between those controlling factors and DOD in
401 CMIP5 models. Figure 6 shows the dominant controlling factors among the three (surface
402 wind speed, bareness, and precipitation) on DOD variations in four seasons from MODIS
403 (left column) and from CMIP5 multi-model mean (right column), respectively. To
404 highlight factors controlling DOD variations near the dust source regions, a mask of
405 AVHRR LAI$\leq$ 0.5 is applied to both coefficients.
406 Bareness plays the most important role in many dusty regions in observations,
407 e.g., over Australia, central U.S., and South America (Figs. 6a-d). Note that while
408 bareness plays an important role over the Sahel during DJF and MAM, it also shows
409 strong signal over some areas in the northern North Africa (Figs. 6a-b). The reliability of

410 this information is limited by the accuracy of LAI retrieval in these areas. The value of
411 bareness in this region is actually quite high (as LAI is very low), but still has weak
412 interannual variability (Figures S6 in the Supplement). Over some areas of North and
413 South Africa, the Middle East, and East Asia, surface wind and precipitation are also
414 quite important.

415 The role of bareness is largely underestimated in CMIP5 models, while surface
416 wind and precipitation become the dominant factors (Figs. 6e-h). The misrepresentation
417 of the connection between DOD and these controlling factors may cause the
418 misrepresentation of the dust load and its variability. Taking Australia for an example,
419 the overestimation of DOD magnitudes may be related to an overestimation of the
420 influence of surface wind on DOD and a lack of constraints from surface bareness.

421 Despite the large differences between the observed and modeled connections
422 between DOD and the controlling factors, some regions show similarities. For instance,
423 over North Africa in DJF, both show an important influence from surface winds (Figs.
424 6a, e), although the locations of surface wind-dominant areas are not exactly the same.
425 Evan et al. (2016) also found a dominant role of surface wind on African dust variability,
426 but they focused on monthly means, not seasonal averages. In MAM, precipitation starts
427 to play a role in some parts of North Africa, while surface wind still dominates in some
428 areas (Fig. 6b). Same increasing influence of precipitation is shown in the multi-model
429 mean, but such an influence seems overestimated (Fig. 6f). In JJA, the influences of
430 precipitation and bareness over the eastern Arabian Peninsula in the multi-model mean
431 (Fig. 6g) also show some similarity to observation (Fig. 6c), although an underestimation
432 of the influence from bareness and an overestimation of precipitation are still there.

433 Also, note that in CMIP5 models, due to lack of constraints from low surface
434 temperature (e.g., over frozen land) and snow cover on dust emission or
435 misrepresentations of dust transport, DOD and also the regression coefficients still exist
436 over NH high latitudes in boreal winter and spring in the multi-model mean (Figs. 6e-f).
437
438 **3.3 Future projections**
439 How will DOD change in response to increasing greenhouse gases? The results
440 from CMIP5 multi-model mean are shown in Figure 7. We compare the DOD during the
441 late half of the 21st century under the RCP 8.5 scenario with that in the historical level
442 (1861-2005 average).
443 Over land, CMIP5 model projects a decrease of global mean DOD in all seasons
444 except JJA (Figs. 7a-d). The inter-model standard deviation is much greater than the
445 multi-model mean, suggesting large discrepancies among individual models. The
446 projected decrease is largely over northern North America, southern North Africa, eastern
447 central Africa, and East Asia, while the increase is largely over northern North Africa, the
448 Middle East, southern North America, South Africa, South America, and southern
449 Australia (Fig. 7). Regional means of DOD change (in percentage) with reference to
450 CMIP5 historical run are summarized in Table 3.
451 What might be the causes of DOD change? Figure 8 shows the projected change
452 of precipitation, bareness, and surface wind speed from CMIP5 multi-model mean. These
453 factors play important role in DOD variations in the present day, although models tend to
454 underestimate the role of bareness and overestimate the influences of precipitation and
455 surface wind (Fig. 6). Increases in precipitation can increase soil moisture and remove

456 airborne dust, thus usually favors a decrease of DOD. As shown in Figs. 8a-d, the
457 increases of precipitation in northern Eurasia, northern North America, the Congo basin
458 in Africa, and Australia (DJF and MAM) may contribute to the decrease of DOD in these
459 regions, while the decreases of precipitation over northern North Africa and the Middle
460 East (DJF and MAM), South Africa, and South America may contribute to the increase of
461 DOD (DJF-SON). Also note that in JJA both precipitation and DOD increase over
462 northern North Africa and the Middle East (Fig. 8c), suggesting other factors dominate
463 the variation of DOD in the multi-model mean.

464 A decrease (increase) of bareness indicates a growth (decay) of vegetation and is
465 usually associated with a decrease (increase) of DOD. In general, except regions such as
466 southern North America, South America, South Africa, part of northern Eurasia, and
467 central Sahel, the pattern of bareness change does not resemble DOD change (Figs. 8e-h).
468 This is probably due to the fact that the overall influence of bareness on DOD variation is
469 underestimated in CMIP5 models (Fig. 6).

470 Increases in surface wind can enhance dust emission and transport, and vise versa.
471 The changes of surface wind in DJF and MAM are similar and likely to contribute to the
472 increase of DOD over northern North Africa, the Middle East, eastern South America,
473 southern South Africa, and southern Australia (Figs. 8i-j). The decrease of DOD over
474 northwestern North America, the Sahel, and northern Australia may also relate to the
475 decrease of surface wind there, in addition to an increase of precipitation and a reduction
476 of bareness. In JJA and SON (Figs. 8k-l), the increases of surface wind in South America,
477 South Africa, central Australia and the decreases of wind in northwestern North America,
478 northern Eurasia, and the central Sahel are also consistent with patterns of DOD change.

In short, variations of CMIP5 DOD in the late half of the 21st century are more consistent with changes of precipitation and surface wind speed than with surface bareness, consistent with the analysis above regarding to the present-day condition.

Here we also present the projected change of DOD from the regression model in Figure 9. The regression model (see section 2.4 for details) is developed based on observed relationships between MODIS DOD and local controlling factors and can largely capture the interannual variations of DOD in the present-day climate (Table S1 in the Supplement). Assuming that the observed connection between DOD and these controlling factors do not change dramatically in the future, we can use this regression model and CMIP5-model projected change of controlling factors to project DOD variations. Compared to DOD projection from CMIP5 models, this approach utilizes additionally observational constrains and is likely to provide a more reliable future projection. We use projected changes of precipitation, bareness, and surface wind speed from seven CMIP5 models with interactive dust emission scheme (see methodology). A similar method is applied to the model output from 16 CMIP5 models, and results are similar (Figure S7 in the Supplement). A mask of present-day LAI ≤ 0.5 is also applied to highlight the changes of DOD near dust source regions. By doing this, we assume the location of major dust sources will not change much at the late half of the 21st century. The unmasked figure is presented in the supplementary file (Figure S8 in the Supplement). The reason we did not use the projected future LAI as a mask is that there're large uncertainties associated with LAI projection, especially over northern hemisphere subtropical regions (e.g., Figs. 8e-h).

In DJF, regression model projected change of DOD over Mexico, North Africa, the Middle East and part of northern China (Fig. 9a) are similar to those projected by CMIP5 models over those dust source regions (Fig. 7a), but with a greater magnitude. In MAM, a decrease of DOD is projected over large area of North Africa (Fig. 9b), which is different from the pattern projected from the CMIP5 multi-model mean (Fig. 7b). The decrease of DOD over northern central U.S. is also different from the overall increase projected by CMIP5 DOD. However, the increase of DOD over the Middle East and the decrease of DOD over northern China are similar to that of CMIP5 DOD. During JJA and SON, DOD decreases over the Sahel and northern China but increases over a belt to the north of central Sahel and parts of the Middle East (Figs. 9c-d). The weak increase of DOD over the southern corner of South Africa in JJA and a slight decrease in SON also has high agreement among the regression projections (dotted areas in Figs. 9c-d). Changes of DOD over Australia are very small in all seasons and show little consistency among the regression projections.

The regression model projection using 16-model output shows very similar patterns (Figure S7 in the Supplement), largely because the projected changes of precipitation, surface wind speed, and bareness from 16-model ensemble mean are similar to those from 7-model ensemble mean in dusty regions (Figure S9 in the Supplement). But there are also some discrepancies in terms of magnitude and pattern that are revealed in the projected DOD patterns, e.g., the projected reduction of DOD is greater and more widespread over the northern Asia in MAM if using 16-model output and the increase of DOD along the southern edge of the Sahara is weaker in JJA and SON (Fig. S7 in the Supplement vs. Fig. 9).

524 The contribution of each controlling factor to the total DOD change is shown in
525 Figure 10. While changes of bareness over North Africa and northern China play an
526 important role in DOD change, changes of precipitation, e.g. over northwestern China in
527 MAM, and surface wind, e.g., over northern North Africa and the Middle East in DJF and
528 MAM, also play vital roles.

529 Both projections from the CMIP5 models and that from the regression model have
530 some uncertainties. The reliability of future projection by CMIP5 models is limited by
531 models' capability of capturing present-day climatology and observed connection
532 between DOD and local controlling factors. As discussed earlier, the overall performance
533 of models is better in those very dusty regions in the NH, such as North Africa and the
534 Middle East, than other regions. Multi-model mean also overestimates the connection
535 between DOD and precipitation and surface wind and underestimates the influence of
536 bareness in the present-day (Fig. 6), which can cast doubts on the projected variation of
537 DOD in response to climate change.

538 The uncertainties associated with regression model are two folds. First, there're
539 uncertainties associated with the regression model itself. Since the regression coefficients
540 are derived from observed relationships between DOD and controlling factors in a
541 relatively short time period, factors controlling the low frequency variation of DOD (e.g.,
542 decadal variations) may not be included. Other meteorological factors that could play an
543 important role in regional dust variability, e.g., nocturnal low-level jets (e.g., Todd et al.,
544 2008; Fiedler et al., 2013; Fiedler et al., 2016) and haboobs over Africa (e.g., Ashpole
545 and Washington, 2013), are not directly considered in the model. The influences of
546 anthropogenic land use/land cover change are also not included in the regression model.

Anthropogenic land use/land cover change has been found to have played an important role in long-term dust variability in some regions (e.g., Neff et al., 2005; 2008; Moulin and Chiapello, 2006; McConnell et al., 2007), although previous modeling study found its influences on future dust emission was minor compared to climate change (Tegen et al., 2004). So the projection made by the regression model only reveals the change of DOD in association with climate change. Second, uncertainties associated with model projected change of controlling factors, such as bareness in U.S. in JJA as pointed by Pu and Ginoux (2017), also limit the accuracy of the results.

Despite these uncertainties, both methods make similar projections particularly in some dusty regions. For instance, the DOD pattern over North Africa in DJF and JJA, an increase of DOD in the central Arabian Peninsula in all seasons, and a decrease of DOD over northern China from MAM to SON (Figs. 7, 9).

4. Discussion

We examined DOD in seven CMIP5 models with interactive dust emission schemes. Other important variables that influence the radiative property of dust, such as Angström exponent and single scattering albedo, are also worth further examination, if these variables are archived. A better quantification of the radiative forcing of dust may also require an examination on the size distribution of dust particles, as studies (e.g., Kok et al., 2017) found in current AeroCom models fraction of coarse dust particles were underestimated and so was the warming effect of dust. Whether this is the case in the CMIP5 models is not clear.

569 Also note that since DOD is an integrated variable, it does not reflect the vertical
570 distribution of dust aerosols. As pointed by Huneeus et al., (2016), dust models with
571 similar performance in simulating aerosol optical depth may have quite large differences
572 in simulating vertical distribution, emission, deposition, and surface concentration of
573 dust. An overall evaluation of dust modeling capability will require detailed examination
574 of these variables and the life cycle of dust in CMIP5 models in addition to DOD.

575 Early studies on future dust projection used offline dust models driven by climate
576 model output under different scenarios. For instance, Mahowald and Luo (2003) used an
577 offline dust model and output from National Center of Atmospheric Research's coupled
578 Climate System Model (CSM) 1.0 (Boville and Gent, 1998) under A1 scenario
579 (Houghton et al., 2001) and projected a decrease of dust emission by the end of the 21st
580 century by -20% to -63%, depending on different scenarios. In general, when they
581 included vegetation change, the projected dust reduction became greater, but including
582 land use change slightly weakened such reduction. Similarly, Tegen et al. (2004) used
583 output from ECHAM4 and HadCM3 and a dust model (Tegen et al., 2002) to examine
584 the change of dust emission by 2040-2050 and 2070-2080 and found results were model
585 and scenario dependent, from -26% to 10%. However, including anthropogenic
586 cultivation practices tended to increase dust emission in both models. They also pointed
587 out that such an influence from anthropogenic land-use was not big enough to overcome
588 the effect of climate change.

589 The interactive dust emission schemes and new generations of climate models
590 used in CMIP5 are likely to provide more reliable projections, but this may also depend
591 on how changes of dust and its radiative forcing are fed back to the climate system in the

592 models. While these projections are largely model-dependent, based on our analysis on
593 the DOD climatology in CMIP5 models, the multi-model mean has a better chance to
594 provide a more reliable projection than individual models.

595 Here a regression model combined with MODIS DOD is used to identify key
596 local factors that control the variation of DOD on the interannual time scale. The results
597 are then compared with model output to examine models' capability of capturing
598 observed connections between DOD and controlling factors. This method may be applied
599 to other dust model intercomparison projects as well, such as AeroCom (Huneeus et al.
600 2011), to help examine model performance.

601

602 **5. Conclusion**

603 Dust aerosol plays an important role in the climate system by directly scattering
604 and absorbing solar and longwave radiation and indirectly affecting the formation and
605 radiative properties of cloud. It is thus very important to understand how well dust is
606 simulated in the state-of-the-art climate models. While many features and variables are
607 systematically examined in the CMIP5 multi-model output, we found that to our best
608 knowledge an evaluation of global dust modeling in CMIP5 models is still in blank. In
609 this study we examined a key variable associated with dust radiative effect, dust optical
610 depth (DOD), using seven CMIP5 models with interactive dust emission schemes and
611 DOD retrieved from MODIS Deep Blue aerosol products.

612 We found that the global spatial pattern and magnitude are largely captured by
613 CMIP5 models in the 2004-2016 climatology, with an underestimation of global DOD
614 (over land) by -25.2% in MAM to -6.4% in DJF. The spatial pattern is better captured in

615 boreal dusty seasons during MAM and JJA. In JJA, the simulated zonal mean DOD from
616 multi-model mean largely resembles MODIS DOD.

617 The magnitudes of multi-model mean are closer to MODIS climatology than most
618 individual models and are largely within ± one order of magnitude of MODIS DOD in
619 the nine regions examined here (North Africa, the Middle East, northern China, North
620 America, India, southeastern Asia, South Africa, South America, and Australia; see Fig. 1
621 and Table 2 for domains). While some models underestimate DOD in North America and
622 South America by more than two orders of magnitude, a few also overestimate DOD in
623 Australia by more than one order of magnitude. Both the magnitude and spatial patterns
624 of DOD are better captured over North Africa and the Middle East than other regions.

625 The multi-model mean also largely captures the seasonal cycle of DOD in some
626 very dusty regions, such as North Africa and the Middle East. Seasonal variations in
627 North America and India are also generally captured by the multi-model mean, with the
628 modeled DOD peaking at approximately the same season as in MODIS DOD, but not so
629 in northern China and southeastern Asia. Seasonal cycles in those dusty regions in the
630 southern hemisphere is generally not well captured, with modeled DOD over South
631 Africa and South America peaking later than that in MODIS DOD but earlier in
632 Australia.

633 The interannual variations of DOD are not captured by most of the CMIP5
634 models during 2004-2016. Models also underestimate the constraints from surface
635 bareness on the variations of DOD and overestimate the influences from surface wind
636 speed and precipitation in those major dust source regions. CMIP5 model projected
637 change of DOD in the late half of the 21st century (under the RCP 8.5 scenario) with

638 reference to historical condition (1861-2005) also shows greater influence from
639 precipitation and surface wind change than from surface bareness. Overall, multi-model
640 mean projects a change of DOD over land from -3.8% in SON to 3.3% in JJA.

641 We also provide a projection of future DOD change using a regression model
642 based on local controlling factors such as surface wind, bareness, and precipitation (Pu
643 and Ginoux, 2017). This model can largely capture the interannual variations of MODIS
644 DOD in 2004-2016. The regression model projects a reduction of DOD in the Sahel in all
645 seasons in the late half of the 21st century under the RCP 8.5 scenario, largely due to a
646 decrease of surface bareness. DOD is projected to increase over the southern edge of the
647 Sahara in association with surface wind and precipitation changes except in MAM, when
648 a reduction of DOD over most part of North Africa is projected. DOD is also projected
649 to increase over the central Arabian Peninsula in all seasons and to decrease over
650 northern China from MAM to SON.

651 Despite large uncertainties associated with both projections, we find some
652 similarities between the two, which adds to the confidence of projected DOD change in
653 these regions, for instance, changes of DOD over North Africa in DJF and JJA, an
654 increase of DOD in the central Arabian Peninsula in all seasons, and a decrease of DOD
655 over northern China from MAM to SON.

656

657

658

659

660

Acknowledgements.

This research is supported by NOAA and Princeton University's Cooperative Institute for Climate Science and NASA under grants NNH14ZDA001N-ACMAP and NNH16ZDA001N-MAP. The authors thank Drs. Songmiao Fan and Fabien Paulot for their helpful comments on the early version of this paper. The insightful comments from two anonymous reviewers improved the paper. We also thank the AERONET program for establishing and maintaining the sunphotometer sites used in this study.

PRECL Precipitation data are provided by the NOAA/OAR/ESRL PSD, Boulder, Colorado, USA, from their web site at *http://www.esrl.noaa.gov/psd/*. The CALIOP products are downloaded from *https://www-calipso.larc.nasa.gov/tools/data_avail/dpo_read.php?y=2007&m=08&d=10*. AVHRR leaf area index data are available at: https://www.ngdc.noaa.gov/docucomp/page?xml=NOAA/NESDIS/NCDC/Geoportal/iso/xml/C00898.xml&view=getDataView&header=none. The ERA-Interim is downloaded from http://www.ecmwf.int/en/research/climate-reanalysis/era-interim. The AERONET coarse mode aerosol optical depth data are downloaded from https://aeronet.gsfc.nasa.gov/. CMIP5 data are downloaded from: https://pcmdi.llnl.gov/projects/esgf-llnl/.

684

685 Reference

686

687 Abudu, S., Cui, C. L., King, J. P., Moreno, J., and Bawazir, A. S.: Modeling of daily pan
688 evaporation using partial least squares regression, Sci China Technol Sc, 54, 163-
689 174, 10.1007/s11431-010-4205-z, 2011.

690 Arora, V. K., Scinocca, J. F., Boer, G. J., Christian, J. R., Denman, K. L., Flato, G. M.,
691 Kharin, V. V., Lee, W. G., and Merryfield, W. J.: Carbon emission limits required
692 to satisfy future representative concentration pathways of greenhouse gases,
693 Geophys Res Lett, 38, 10.1029/2010gl046270, 2011.

694 Ashpole, I., and Washington, R.: A new high-resolution central and western Saharan
695 summertime dust source map from automated satellite dust plume tracking, J
696 Geophys Res-Atmos, 118, 6981-6995, 10.1002/jgrd.50554, 2013.

697 Baddock, M. C., Ginoux, P., Bullard, J. E., and Gill, T. E.: Do MODIS-defined dust
698 sources have a geomorphological signature?, Geophys Res Lett, 43, 2606-2613,
699 10.1002/2015gl067327, 2016.

700 Bangert, M., Nenes, A., Vogel, B., Vogel, H., Barahona, D., Karydis, V. A., Kumar, P.,
701 Kottmeier, C., and Blahak, U.: Saharan dust event impacts on cloud formation
702 and radiation over Western Europe, Atmos Chem Phys, 12, 4045-4063,
703 10.5194/acp-12-4045-2012, 2012.

704 Bellouin, N., Rae, J., Jones, A., Johnson, C., Haywood, J., and Boucher, O.: Aerosol
705 forcing in the Climate Model Intercomparison Project (CMIP5) simulations by
706 HadGEM2-ES and the role of ammonium nitrate, J Geophys Res-Atmos, 116,
707 10.1029/2011jd016074, 2011.

708 Bentsen, M., Bethke, I., Debernard, J. B., Iversen, T., Kirkevag, A., Seland, O., Drange,
709 H., Roelandt, C., Seierstad, I. A., Hoose, C., and Kristjansson, J. E.: The
710 Norwegian Earth System Model, NorESM1-M - Part 1: Description and basic
711 evaluation of the physical climate, Geosci Model Dev, 6, 687-720, 10.5194/gmd-
712 6-687-2013, 2013.
713 Boville, B. A., and Gent, P. R.: The NCAR Climate System Model, version one, J
714 Climate, 11, 1115-1130, Doi 10.1175/1520-
715 0442(1998)011<1115:Tncsmv>2.0.Co;2, 1998.
716 Chen, M. Y., Xie, P. P., Janowiak, J. E., and Arkin, P. A.: Global land precipitation: A
717 50-yr monthly analysis based on gauge observations, J Hydrometeorol, 3, 249-
718 266, Doi 10.1175/1525-7541(2002)003<0249:Glpaym>2.0.Co;2, 2002.
719 Claverie, M., Matthews, J. L., Vermote, E. F., and Justice, C. O.: A 30+ Year AVHRR
720 LAI and FAPAR Climate Data Record: Algorithm Description and Validation,
721 Remote Sens-Basel, 8, 10.3390/rs8030263, 2016.
722 Collins, W. J., Bellouin, N., Doutriaux-Boucher, M., Gedney, N., Halloran, P., Hinton,
723 T., Hughes, J., Jones, C. D., Joshi, M., Liddicoat, S., Martin, G., O'Connor, F.,
724 Rae, J., Senior, C., Sitch, S., Totterdell, I., Wiltshire, A., and Woodward, S.:
725 Development and evaluation of an Earth-System model-HadGEM2, Geosci
726 Model Dev, 4, 1051-1075, 10.5194/gmd-4-1051-2011, 2011.
727 Cook, B. I., Miller, R. L., and Seager, R.: Dust and sea surface temperature forcing of the
728 1930s "Dust Bowl" drought, Geophys Res Lett, 35, 10.1029/2008gl033486, 2008.

729 Cook, B. I., Miller, R. L., and Seager, R.: Amplification of the North American "Dust
730 Bowl" drought through human-induced land degradation, P Natl Acad Sci USA,
731 106, 4997-5001, 10.1073/pnas.0810200106, 2009.
732 Cook, B. I., Seager, R., Miller, R. L., and Mason, J. A.: Intensification of North
733 American Megadroughts through Surface and Dust Aerosol Forcing, J Climate,
734 26, 4414-4430, 10.1175/Jcli-D-12-00022.1, 2013.
735 Croft, B., Lohmann, U., and von Salzen, K.: Black carbon ageing in the Canadian Centre
736 for Climate modelling and analysis atmospheric general circulation model, Atmos
737 Chem Phys, 5, 1931-1949, 2005.
738 Donner, L. J., Wyman, B. L., Hemler, R. S., Horowitz, L. W., Ming, Y., Zhao, M., Golaz,
739 J. C., Ginoux, P., Lin, S. J., Schwarzkopf, M. D., Austin, J., Alaka, G., Cooke, W.
740 F., Delworth, T. L., Freidenreich, S. M., Gordon, C. T., Griffies, S. M., Held, I.
741 M., Hurlin, W. J., Klein, S. A., Knutson, T. R., Langenhorst, A. R., Lee, H. C.,
742 Lin, Y. L., Magi, B. I., Malyshev, S. L., Milly, P. C. D., Naik, V., Nath, M. J.,
743 Pincus, R., Ploshay, J. J., Ramaswamy, V., Seman, C. J., Shevliakova, E., Sirutis,
744 J. J., Stern, W. F., Stouffer, R. J., Wilson, R. J., Winton, M., Wittenberg, A. T.,
745 and Zeng, F. R.: The Dynamical Core, Physical Parameterizations, and Basic
746 Simulation Characteristics of the Atmospheric Component AM3 of the GFDL
747 Global Coupled Model CM3, J Climate, 24, 3484-3519, 10.1175/2011jcli3955.1,
748 2011.
749 Dunion, J. P., and Velden, C. S.: The impact of the Saharan air layer on Atlantic tropical
750 cyclone activity, B Am Meteorol Soc, 85, 353-+, 10.1175/Bams-85-3-353, 2004.

751 Evan, A. T., Dunion, J., Foley, J. A., Heidinger, A. K., and Velden, C. S.: New evidence
752 for a relationship between Atlantic tropical cyclone activity and African dust
753 outbreaks, Geophys Res Lett, 33, 10.1029/2006gl026408, 2006.
754 Evan, A. T., and Mukhopadhyay, S.: African Dust over the Northern Tropical Atlantic:
755 1955-2008, J Appl Meteorol Clim, 49, 2213-2229, 10.1175/2010jamc2485.1,
756 2010.
757 Evan, A. T., Flamant, C., Fiedler, S., and Doherty, O.: An analysis of aeolian dust in
758 climate models, Geophys Res Lett, 41, 5996-6001, 10.1002/2014gl060545, 2014.
759 Evan, A. T., Flamant, C., Gaetani, M., and Guichard, F.: The past, present and future of
760 African dust, Nature, 531, 493-+, 10.1038/nature17149, 2016.
761 Evans, S., Ginoux, P., Malyshev, S., and Shevliakova, E.: Climate-vegetation interaction
762 and amplification of Australian dust variability, Geophys Res Lett, 43, 11823-
763 11830, 10.1002/2016gl071016, 2016.
764 Fecan, F., Marticorena, B., and Bergametti, G.: Parametrization of the increase of the
765 aeolian erosion threshold wind friction velocity due to soil moisture for arid and
766 semi-arid areas, Ann Geophys-Atm Hydr, 17, 149-157, DOI
767 10.1007/s005850050744, 1999.
768 Fiedler, S., Schepanski, K., Heinold, B., Knippertz, P., and Tegen, I.: Climatology of
769 nocturnal low-level jets over North Africa and implications for modeling mineral
770 dust emission, J Geophys Res-Atmos, 118, 6100-6121, 10.1002/jgrd.50394, 2013.
771 Fiedler, S., Knippertz, P., Woodward, S., Martin, G. M., Bellouin, N., Ross, A. N.,
772 Heinold, B., Schepanski, K., Birch, C. E., and Tegen, I.: A process-based

773 evaluation of dust-emitting winds in the CMIP5 simulation of HadGEM2-ES,
774 Clim Dynam, 46, 1107-1130, 10.1007/s00382-015-2635-9, 2016.
775 Fung, I. Y., Meyn, S. K., Tegen, I., Doney, S. C., John, J. G., and Bishop, J. K. B.: Iron
776 supply and demand in the upper ocean, Global Biogeochem Cy, 14, 281-295, Doi
777 10.1029/1999gb900059, 2000.
778 Fuss, S., Canadell, J. G., Peters, G. P., Tavoni, M., Andrew, R. M., Ciais, P., Jackson, R.
779 B., Jones, C. D., Kraxner, F., Nakicenovic, N., Le Quere, C., Raupach, M. R.,
780 Sharifi, A., Smith, P., and Yamagata, Y.: COMMENTARY: Betting on negative
781 emissions, Nat Clim Change, 4, 850-853, DOI 10.1038/nclimate2392, 2014.
782 Gillette, D. A., and Passi, R.: Modeling Dust Emission Caused by Wind Erosion, J
783 Geophys Res-Atmos, 93, 14233-14242, DOI 10.1029/JD093iD11p14233, 1988.
784 Ginoux, P., Chin, M., Tegen, I., Prospero, J. M., Holben, B., Dubovik, O., and Lin, S. J.:
785 Sources and distributions of dust aerosols simulated with the GOCART model, J
786 Geophys Res-Atmos, 106, 20255-20273, Doi 10.1029/2000jd000053, 2001.
787 Ginoux, P., Garbuzov, D., and Hsu, N. C.: Identification of anthropogenic and natural
788 dust sources using Moderate Resolution Imaging Spectroradiometer (MODIS)
789 Deep Blue level 2 data, J Geophys Res-Atmos, 115, 10.1029/2009jd012398,
790 2010.
791 Ginoux, P., Clarisse, L., Clerbaux, C., Coheur, P. F., Dubovik, O., Hsu, N. C., and Van
792 Damme, M.: Mixing of dust and NH3 observed globally over anthropogenic dust
793 sources, Atmos Chem Phys, 12, 7351-7363, 10.5194/acp-12-7351-2012, 2012a.
794 Ginoux, P., Prospero, J. M., Gill, T. E., Hsu, N. C., and Zhao, M.: Global-Scale
795 Attribution of Anthropogenic and Natural Dust Sources and Their Emission Rates

796 Based on MODIS Deep Blue Aerosol Products, Rev Geophys, 50,
797 10.1029/2012rg000388, 2012b.
798 Houghton, J., Ding, Y., Griggs, D. J., Noguer, M., Linden, P. J. v. d., Dai, X., Maskell,
799 K., and Johnson, C. A.: Climate Change 2001: The scientific basis. Contribution
800 of Working Group I to the Third Assessment Report of the Intergovernmental
801 Panel on Climate Change, in, Cambridge Univ. Press, Cambridge, UK, 2001.
802 Hsu, N. C., Tsay, S. C., King, M. D., and Herman, J. R.: Aerosol properties over bright-
803 reflecting source regions, Ieee T Geosci Remote, 42, 557-569,
804 10.1109/Tgrs.2004.824067, 2004.
805 Hsu, N. C., Tsay, S. C., King, M. D., and Herman, J. R.: Deep blue retrievals of Asian
806 aerosol properties during ACE-Asia, Ieee T Geosci Remote, 44, 3180-3195,
807 10.1109/Tgrs.2006.879540, 2006.
808 Hsu, N. C., Jeong, M. J., Bettenhausen, C., Sayer, A. M., Hansell, R., Seftor, C. S.,
809 Huang, J., and Tsay, S. C.: Enhanced Deep Blue aerosol retrieval algorithm: The
810 second generation, J Geophys Res-Atmos, 118, 9296-9315, 10.1002/jgrd.50712,
811 2013.
812 Huneeus, N., Schulz, M., Balkanski, Y., Griesfeller, J., Prospero, J., Kinne, S., Bauer, S.,
813 Boucher, O., Chin, M., Dentener, F., Diehl, T., Easter, R., Fillmore, D., Ghan, S.,
814 Ginoux, P., Grini, A., Horowitz, L., Koch, D., Krol, M. C., Landing, W., Liu, X.,
815 Mahowald, N., Miller, R., Morcrette, J. J., Myhre, G., Penner, J., Perlwitz, J.,
816 Stier, P., Takemura, T., and Zender, C. S.: Global dust model intercomparison in
817 AeroCom phase I, Atmos Chem Phys, 11, 7781-7816, 10.5194/acp-11-7781-
818 2011, 2011.

819 Jickells, T. D., An, Z. S., Andersen, K. K., Baker, A. R., Bergametti, G., Brooks, N., Cao,
820 J. J., Boyd, P. W., Duce, R. A., Hunter, K. A., Kawahata, H., Kubilay, N.,
821 laRoche, J., Liss, P. S., Mahowald, N., Prospero, J. M., Ridgwell, A. J., Tegen, I.,
822 and Torres, R.: Global iron connections between desert dust, ocean
823 biogeochemistry, and climate, Science, 308, 67-71, DOI
824 10.1126/science.1105959, 2005.
825 Jin, Q., Wei, J., Yang, Z. L., Pu, B., and Huang, J.: Consistent response of Indian summer
826 monsoon to Middle East dust in observations and simulations, Atmos Chem Phys,
827 15, 9897-9915, 10.5194/acp-15-9897-2015, 2015.
828 Jin, Q. J., Wei, J. F., and Yang, Z. L.: Positive response of Indian summer rainfall to
829 Middle East dust, Geophys Res Lett, 41, 4068-4074, 10.1002/2014gl059980,
830 2014.
831 Jin, Q. J., Yang, Z. L., and Wei, J. F.: Seasonal Responses of Indian Summer Monsoon to
832 Dust Aerosols in the Middle East, India, and China, J Climate, 29, 6329-6349,
833 10.1175/Jcli-D-15-0622.1, 2016.
834 Kim, M. K., Lau, W. K. M., Kim, K. M., Sang, J., Kim, Y. H., and Lee, W. S.:
835 Amplification of ENSO effects on Indian summer monsoon by absorbing
836 aerosols, Clim Dynam, 46, 2657-2671, 10.1007/s00382-015-2722-y, 2016.
837 Kok, J. F., Ridley, D. A., Zhou, Q., Miller, R. L., Zhao, C., Heald, C. L., Ward, D. S.,
838 Albani, S., and Haustein, K.: Smaller desert dust cooling effect estimated from
839 analysis of dust size and abundance, Nat Geosci, 10, 274-+, 10.1038/Ngeo2912,
840 2017.

841 Laurent, B., Marticorena, B., Bergametti, G., and Mei, F.: Modeling mineral dust
842 emissions from Chinese and Mongolian deserts, Global Planet Change, 52, 121-
843 141, 10.1016/j.gloplacha.2006.02.012, 2006.
844 Levin, Z., Ganor, E., and Gladstein, V.: The effects of desert particles coated with sulfate
845 on rain formation in the eastern Mediterranean, J Appl Meteorol, 35, 1511-1523,
846 Doi 10.1175/1520-0450(1996)035<1511:Teodpc>2.0.Co;2, 1996.
847 Mahowald, N. M., and Luo, C.: A less dusty future?, Geophys Res Lett, 30,
848 10.1029/2003gl017880, 2003.
849 Mahowald, N. M., Kloster, S., Engelstaedter, S., Moore, J. K., Mukhopadhyay, S.,
850 McConnell, J. R., Albani, S., Doney, S. C., Bhattacharya, A., Curran, M. A. J.,
851 Flanner, M. G., Hoffman, F. M., Lawrence, D. M., Lindsay, K., Mayewski, P. A.,
852 Neff, J., Rothenberg, D., Thomas, E., Thornton, P. E., and Zender, C. S.:
853 Observed 20th century desert dust variability: impact on climate and
854 biogeochemistry, Atmos Chem Phys, 10, 10875-10893, 10.5194/acp-10-10875-
855 2010, 2010.
856 Marticorena, B., and Bergametti, G.: Modeling the Atmospheric Dust Cycle .1. Design of
857 a Soil-Derived Dust Emission Scheme, J Geophys Res-Atmos, 100, 16415-16430,
858 Doi 10.1029/95jd00690, 1995.
859 Marx, S. K., McGowan, H. A., and Kamber, B. S.: Long-range dust transport from
860 eastern Australia: A proxy for Holocene aridity and ENSO-type climate
861 variability, Earth Planet Sc Lett, 282, 167-177, 10.1016/j.epsl.2009.03.013, 2009.
862 McConnell, J. R., Aristarain, A. J., Banta, J. R., Edwards, P. R., and Simoes, J. C.: 20th-
863 Century doubling in dust archived in an Antarctic Peninsula ice core parallels

climate change and desertification in South America, P Natl Acad Sci USA, 104, 5743-5748, 10.1073/pnas.0607657104, 2007.

Miller, R. L., and Tegen, I.: Climate response to soil dust aerosols, J Climate, 11, 3247-3267, Doi 10.1175/1520-0442(1998)011<3247:Crtsda>2.0.Co;2, 1998.

Miller, R. L., Tegen, I., and Perlwitz, J.: Surface radiative forcing by soil dust aerosols and the hydrologic cycle, J Geophys Res-Atmos, 109, 10.1029/2003jd004085, 2004.

Misra, A., Kanawade, V. P., and Tripathi, S. N.: Quantitative assessment of AOD from 17 CMIP5 models based on satellite-derived AOD over India, Ann Geophys-Germany, 34, 657-671, 10.5194/angeo-34-657-2016, 2016.

Moulin, C., and Chiapello, I.: Impact of human-induced desertification on the intensification of Sahel dust emission and export over the last decades, Geophys Res Lett, 33, 10.1029/2006gl025923, 2006.

Myhre, G., Shindell, D., Bréon, F.-M., Collins, W., Fuglestvedt, J., Huang, J., Koch, D., Lamarque, J.-F., Lee, D., Mendoza, B., Nakajima, T., Robock, A., Stephens, G., Takemura, T., and Zhang, H.: Anthropogenic and Natural Radiative Forcing. , in: Climate Change 2013: The Physical Science Basis. Contribution of Working Group I to the Fifth Assessment Report of the Intergovernmental Panel on Climate Change, edited by: Stocker, T. F., Qin, D., Plattner, G.-K., Tignor, M., Allen, S. K., Boschung, J., Nauels, A., Xia, Y., Bex, V., and Midgley, P. M., Cambridge University Press, Cambridge, United Kingdom and New York, NY, USA, 2013.

886 Nakajima, T., Higurashi, A., Kawamoto, K., and Penner, J. E.: A possible correlation
887 between satellite-derived cloud and aerosol microphysical parameters, Geophys
888 Res Lett, 28, 1171-1174, Doi 10.1029/2000gl012186, 2001.
889 Neff, J. C., Reynolds, R. L., Belnap, J., and Lamothe, P.: Multi-decadal impacts of
890 grazing on soil physical and biogeochemical properties in southeast Utah, Ecol
891 Appl, 15, 87-95, Doi 10.1890/04-0268, 2005.
892 Neff, J. C., Ballantyne, A. P., Farmer, G. L., Mahowald, N. M., Conroy, J. L., Landry, C.
893 C., Overpeck, J. T., Painter, T. H., Lawrence, C. R., and Reynolds, R. L.:
894 Increasing eolian dust deposition in the western United States linked to human
895 activity, Nat Geosci, 1, 189-195, 10.1038/ngeo133, 2008.
896 O'Brien, R. M.: A caution regarding rules of thumb for variance inflation factors, Qual
897 Quant, 41, 673-690, 10.1007/s11135-006-9018-6, 2007.
898 O'Neill, N. T., Eck, T. F., Smirnov, A., Holben, B. N., and Thulasiraman, S.: Spectral
899 discrimination of coarse and fine mode optical depth, J Geophys Res-Atmos, 108,
900 10.1029/2002jd002975, 2003.
901 Prospero, J. M., and Nees, R. T.: Impact of the North African Drought and El-Nino on
902 Mineral Dust in the Barbados Trade Winds, Nature, 320, 735-738, DOI
903 10.1038/320735a0, 1986.
904 Prospero, J. M., and Lamb, P. J.: African droughts and dust transport to the Caribbean:
905 Climate change implications, Science, 302, 1024-1027, DOI
906 10.1126/science.1089915, 2003.

907 Pu, B., Fu, R., Dickinson, R. E., and Fernando, D. N.: Why do summer droughts in the
908 Southern Great Plains occur in some La Nina years but not others?, J Geophys
909 Res-Atmos, 121, 1120-1137, 10.1002/2015jd023508, 2016.
910 Pu, B., and Ginoux, P.: The impact of the Pacific Decadal Oscillation on springtime dust
911 activity in Syria, Atmos Chem Phys, 16, 13431-13448, 10.5194/acp-16-13431-
912 2016, 2016.
913 Pu, B., and Ginoux, P.: Projection of American dustiness in the late 21st century due to
914 climate change, Scientific reports, 7, 10.1038/s41598-017-05431-9, 2017.
915 Reader, M. C., Fung, I., and McFarlane, N.: The mineral dust aerosol cycle during the
916 last glacial maximum (vol 104, pg 9381, 1999), J Geophys Res-Atmos, 104,
917 22319-22320, Doi 10.1029/1999jd900434, 1999.
918 Riahi, K., Rao, S., Krey, V., Cho, C. H., Chirkov, V., Fischer, G., Kindermann, G.,
919 Nakicenovic, N., and Rafaj, P.: RCP 8.5-A scenario of comparatively high
920 greenhouse gas emissions, Climatic Change, 109, 33-57, 10.1007/s10584-011-
921 0149-y, 2011.
922 Rosenfield, J. E., Considine, D. B., Meade, P. E., Bacmeister, J. T., Jackman, C. H., and
923 Schoeberl, M. R.: Stratospheric effects of Mount Pinatubo aerosol studied with a
924 coupled two-dimensional model, J Geophys Res-Atmos, 102, 3649-3670, Doi
925 10.1029/96jd03820, 1997.
926 Sanap, S. D., Ayantika, D. C., Pandithurai, G., and Niranjan, K.: Assessment of the
927 aerosol distribution over Indian subcontinent in CMIP5 models, Atmospheric
928 Environment, 87, 123-137, 10.1016/j.atmosenv.2014.01.017, 2014.

929 Seland, O., Iversen, T., Kirkevag, A., and Storelvmo, T.: Aerosol-climate interactions in
930 the CAM-Oslo atmospheric GCM and investigation of associated basic
931 shortcomings, Tellus A, 60, 459-491, 10.1111/j.1600-0870.2008.00318.x, 2008.
932 Shao, Y. P., Wyrwoll, K. H., Chappell, A., Huang, J. P., Lin, Z. H., McTainsh, G. H.,
933 Mikami, M., Tanaka, T. Y., Wang, X. L., and Yoon, S.: Dust cycle: An emerging
934 core theme in Earth system science, Aeolian Res, 2, 181-204,
935 10.1016/j.aeolia.2011.02.001, 2011.
936 Sharma, D., and Miller, R. L.: Revisiting the observed correlation between weekly
937 averaged Indian monsoon precipitation and Arabian Sea aerosol optical depth,
938 Geophys Res Lett, 44, 10006-10016, 10.1002/2017gl074373, 2017.
939 Shindell, D. T., Lamarque, J. F., Schulz, M., Flanner, M., Jiao, C., Chin, M., Young, P. J.,
940 Lee, Y. H., Rotstayn, L., Mahowald, N., Milly, G., Faluvegi, G., Balkanski, Y.,
941 Collins, W. J., Conley, A. J., Dalsoren, S., Easter, R., Ghan, S., Horowitz, L., Liu,
942 X., Myhre, G., Nagashima, T., Naik, V., Rumbold, S. T., Skeie, R., Sudo, K.,
943 Szopa, S., Takemura, T., Voulgarakis, A., Yoon, J. H., and Lo, F.: Radiative
944 forcing in the ACCMIP historical and future climate simulations, Atmos Chem
945 Phys, 13, 2939-2974, 10.5194/acp-13-2939-2013, 2013.
946 Solmon, F., Nair, V. S., and Mallet, M.: Increasing Arabian dust activity and the Indian
947 summer monsoon, Atmos Chem Phys, 15, 8051-8064, 10.5194/acp-15-8051-
948 2015, 2015.
949 Strong, J. D., Vecchi, G. A., and Ginoux, P.: The Climatological Effect of Saharan Dust
950 on Global Tropical Cyclones in a Fully Coupled GCM, Journal of Geophysical
951 Research - Atmospheres, 123, https://doi.org/10.1029/2017JD027808, 2018.

952 Strong, J. D. O., Vecchi, G. A., and Ginoux, P.: The Response of the Tropical Atlantic
953 and West African Climate to Saharan Dust in a Fully Coupled GCM, J Climate,
954 28, 7071-7092, 10.1175/Jcli-D-14-00797.1, 2015.
955 Sun, D. L., Lau, K. M., and Kafatos, M.: Contrasting the 2007 and 2005 hurricane
956 seasons: Evidence of possible impacts of Saharan dry air and dust on tropical
957 cyclone activity in the Atlantic basin, Geophys Res Lett, 35,
958 10.1029/2008gl034529, 2008.
959 Takemura, T., Okamoto, H., Maruyama, Y., Numaguti, A., Higurashi, A., and Nakajima,
960 T.: Global three-dimensional simulation of aerosol optical thickness distribution
961 of various origins, J Geophys Res-Atmos, 105, 17853-17873, Doi
962 10.1029/2000jd900265, 2000.
963 Tegen, I., Harrison, S. P., Kohfeld, K., Prentice, I. C., Coe, M., and Heimann, M.: Impact
964 of vegetation and preferential source areas on global dust aerosol: Results from a
965 model study, J Geophys Res-Atmos, 107, 10.1029/2001jd000963, 2002.
966 Tegen, I., Werner, M., Harrison, S. P., and Kohfeld, K. E.: Relative importance of
967 climate and land use in determining present and future global soil dust emission,
968 Geophys Res Lett, 31, 10.1029/2003gl019216, 2004.
969 Todd, M. C., Washington, R., Raghavan, S., Lizcano, G., and Knippertz, P.: Regional
970 model simulations of the Bodele low-level jet of northern Chad during the Bodele
971 Dust Experiment (BoDEx 2005), J Climate, 21, 995-1012,
972 10.1175/2007jcli1766.1, 2008.

973 Vinoj, V., Rasch, P. J., Wang, H. L., Yoon, J. H., Ma, P. L., Landu, K., and Singh, B.:
974 Short-term modulation of Indian summer monsoon rainfall by West Asian dust,
975 Nat Geosci, 7, 308-313, 10.1038/ngeo2107, 2014.
976 Watanabe, S., Hajima, T., Sudo, K., Nagashima, T., Takemura, T., Okajima, H., Nozawa,
977 T., Kawase, H., Abe, M., Yokohata, T., Ise, T., Sato, H., Kato, E., Takata, K.,
978 Emori, S., and Kawamiya, M.: MIROC-ESM 2010: model description and basic
979 results of CMIP5-20c3m experiments, Geosci Model Dev, 4, 845-872,
980 10.5194/gmd-4-845-2011, 2011.
981 Winker, D. M., Hunt, W., and Hostetler, C.: Status and performance of the CALIOP
982 lidar, Bba Lib, 5575, 8-15, 10.1117/12.571955, 2004.
983 Winker, D. M., Hunt, W. H., and McGill, M. J.: Initial performance assessment of
984 CALIOP, Geophys Res Lett, 34, 10.1029/2007gl030135, 2007.
985 Wong, S., and Dessler, A. E.: Suppression of deep convection over the tropical North
986 Atlantic by the Saharan Air Layer, Geophys Res Lett, 32, 10.1029/2004gl022295,
987 2005.
988 Wurzler, S., Reisin, T. G., and Levin, Z.: Modification of mineral dust particles by cloud
989 processing and subsequent effects on drop size distributions, J Geophys Res-
990 Atmos, 105, 4501-4512, Doi 10.1029/1999jd900980, 2000.
991 Zender, C. S., and Kwon, E. Y.: Regional contrasts in dust emission responses to climate,
992 J Geophys Res-Atmos, 110, 10.1029/2004jd005501, 2005.
993 Zhao, T. L., Gong, S. L., Zhang, X. Y., Blanchet, J. P., McKendry, I. G., and Zhou, Z. J.:
994 A simulated climatology of Asian dust aerosol and its trans-Pacific transport. Part

I: Mean climate and validation, J Climate, 19, 88-103, Doi 10.1175/Jcli3605.1, 2006.

1000 Table 1 CMIP5 models used in this study. Models tagged with plus signs (+) included
1001 anthropogenic land use/land cover change in their vegetation prediction.
1002
1003 Table 2 List of regions selected to compare model output with MODIS DOD. Locations
1004 of these regions are also plotted in Fig. 1b. Acronyms are used for some regions for short,
1005 and are listed in the brackets in the first column. Note that the region names such as
1006 Northern China and India are not exactly the same as their geographical definitions but
1007 also covers some areas from nearby countries.
1008
1009 Table 3 Changes of DOD in the late half of the 21st century (2051-2100; RCP 8.5
1010 scenario) from the historical condition (1861-2005) projected by CMIP5 multi-model
1011 mean (second to fifth columns) and the regression model (sixth to ninth columns) in the
1012 nine regions. Changes of DOD are shown in percentage with reference to CMIP5 multi-
1013 model historical run. Note that in some regions the projected change by the regression
1014 model is quite large (i.e., greater than ± 100%), largely due to the underestimation of
1015 CMIP5 historical run in these regions.
1016
1017
1018
1019
1020
1021
1022

1023 Figure 1. Figure 1. Climatology (2004-2016) of Aqua and Terra combined DOD (i.e.,
1024 MODIS DOD; top panel) and multi-model mean of CMIP5 DOD (bottom) for four
1025 seasons. The pattern correlation (centered; calculated after interpolating MODIS DOD to
1026 CMIP5 DOD grids) between CMIP5 and MODIS DOD are shown in pink in the bottom
1027 panel. Blue numbers denote global mean DOD over land. For CMIP5 model results, ±
1028 one standard deviation among seven CMIP5 models is also shown. Black boxes in (b)
1029 denote nine averaging regions (Table 2). Here we only added these boxes in (b) instead of
1030 every plot to keep the figure clean. Note that CMIP5 multi-model mean is masked by
1031 MODIS DOD for comparison. Dotted area in (e)-(h) shows where multi-model mean is
1032 greater than one inter-model standard deviation.
1033
1034 Figure 2. Zonal mean DOD from MODIS (thick red), CMIP5 multi-model mean (thick
1035 black), and each individual model (other colorful lines).
1036
1037 Figure 3. Seasonal cycle of DOD in nine regions (Table 2) averaged over 2004-2016.
1038 Thick red lines denote MODIS DOD, thick black lines denote CMIP5 multi-model mean,
1039 and other colorful lines denote individual model output. The annual means from MODIS
1040 DOD (Obs; red) and multi-model mean (Ens; black) are shown in each panel. Note that in
1041 (i) MODIS DOD (red line) is scaled ten times to better display the season cycle.
1042
1043 Figure 4. Spatial statistics comparing DOD from CMIP5 models with that from MODIS
1044 in nine regions. Label on the X-axis shows individual models (1-7) and multi-model
1045 mean (8). Y-axis shows the ratio of pattern standard deviations between model

1046 climatology (2004-2016) and that of MODIS, which reveals the relative amplitude of the
1047 simulated DOD versus satellite DOD. The color denotes pattern correlation (centered)
1048 between each model and MODIS DOD in each region.
1049
1050 Figure 5. Correlations (color) between regional averaged time series from CMIP5 DOD
1051 and MODIS DOD from 2004 to 2016 for four seasons. Numbers in the X-axis denotes
1052 each model (1-7) and multi-model mean (8). Correlations significant at the 90%
1053 confidence level are marked by a star and significance at the 95% confidence level by
1054 two stars.
1055
1056 Figure 6. Regression coefficients calculated by regressing DOD in each season onto
1057 standardized precipitation (purple), bareness (orange), and surface wind speed (green)
1058 from 2004 to 2016. Coefficients obtained using MODIS DOD and observed controlling
1059 factors (interpolated to a 2° by 2.5° grid) and those using CMIP5 multi-model mean DOD
1060 and controlling factors are shown in the left and right columns, respectively. The color of
1061 the shading denotes the largest coefficient in absolute value among the three, while the
1062 saturation of the color shows the magnitude of the coefficient (from 0 to 0.02). Only
1063 regression coefficients significant at the 90% confidence level (Bootstrap test) are shown.
1064 Missing values are shaded in grey. To highlight coefficients near the source regions, a
1065 mask of LAI $\leq$ 0.5 is applied.
1066
1067 Figure 7. Projected changes of DOD in the late half of the 21st century (under the RCP
1068 8.5 scenario) from that in the historical level (1861-2005) by CMIP5 multi-model mean

1069 for four seasons. The percentage change of global mean (over land) DOD ± one inter-
1070 model standard deviation is shown at the bottom of each plot. Areas with sign agreement
1071 among the models reaches 71.4% (i.e., at least five out of seven models have the same
1072 sign as the multi-model mean) are dotted.
1073
1074 Figure 8. Projected difference of (a)-(d) precipitation (mm day-1), (e)-(h) bareness, and
1075 (i)-(l) 10 m wind (m s-1) between the late half of the 21st century (2051-2100; RCP 8.5
1076 scenario) and historical level (1861-2005) from multi-model mean of seven CMIP5
1077 models. Areas with sign agreement among the models reaches 71.4% (i.e., at least five
1078 out of seven models have the same sign as the multi-model mean) are dotted.
1079
1080 Figure 9. Projected change of DOD in the late half of the 21st century under the RCP 8.5
1081 scenario by the regression model. The results are calculated using the regression
1082 coefficients obtained from observations during 2004-2016 (see methodology) and
1083 projected changes of precipitation, bareness, and surface wind from seven CMIP5
1084 models. Dotted areas are regions with sign agreement among the regression projections
1085 (using output of each of the seven models) above 71.4% (i.e., at least five out of seven
1086 regression projections have the same sign as the multi-model mean projection). To
1087 highlight DOD variations near the source regions, a mask of LAI $\leq$ 0.5 (from present-day
1088 climatology) is applied.
1089
1090 Figure 10. (a)-(d) Projected change of DOD in the late half of the 21st century under the
1091 RCP 8.5 scenario by the regression model and output from seven CMIP5 models (same

as Fig. 9), and contributions from each component, (e)-(h) precipitation, (j)-(i) bareness, and (m)-(p) surface wind speed. Dotted areas are regions with sign agreement among the models above 71.4%. To highlight DOD variations near the source regions, a mask of LAI $\leq$ 0.5 (from present-day climatology) is applied.

Table 1 CMIP5 models used in this study. Models tagged with plus signs (+) included anthropogenic land use/land cover change in their vegetation prediction.

Model	lat/lon resolution	Dust emission implementation	Dynamic Vegetation	Model reference
CanESM2	2.8°×2.8°	Reader et al. (1999); Croft et al. (2005)	N^+	Arora et al. (2011)
GFDL-CM3	2.0°×2.5°	Ginoux et al. (2001)	Y^+	Donner et al. (2011)
HadGEM2-CC	1.2°×1.8°	Marticorena and Bergametti (1995)	Y^+	Collins et al. (2011)
HadGEM2-ES	1.2°×1.8°	Marticorena and Bergametti (1995)	Y^+	Collins et al. (2011)
MIROC-ESM	2.8°×2.8°	Takemura et al. (2000)	Y^+	Watanabe et al. (2011)
MIROC-ESM-CHEM	2.8°×2.8°	Takemura et al. (2000)	Y^+	Watanabe et al. (2011)
NorESM1-M	1.9°×2.5°	Seland et al. (2008)	N^+	Bentsen et al. (2013)

Table 2 List of regions selected to compare model output with MODIS DOD. Locations of these regions are also plotted in Fig. 1b. Acronyms are used for some regions for short, and are listed in the brackets in the first column. Note that the region names such as northern China and India are not exactly the same as their geographical definitions but also cover some areas from nearby countries.

Region	Domain
North Africa (N. Africa)	5°-50°N, 18°W-35°E
Middle East	12°-50°N, 35°-60°E
Northern China (N. China)	35°-50°N, 70°-110°E
North America (N. America)	25°-50°N, 95°-125°W
India	5°-35°N, 60°-90°E
Southeastern Asia (SE. Asia)	9°-35°N, 90°-121°E
South Africa (S. Africa)	15°-35°S, 10°-50°N
South America (S. America)	0°-55°S, 60°-83°W
Australia	10°-40°S, 112°-155°E

Table 3 Changes of DOD in the late half of the 21st century (2051-2100; RCP 8.5 scenario) from the historical condition (1861-2005) projected by CMIP5 multi-model mean (second to fifth columns) and the regression model (sixth to ninth columns) in nine regions. Changes of DOD are shown in percentage with reference to CMIP5 multi-model historical run. Note that in some regions the projected change by the regression model is quite large (i.e., greater than ± 100%), largely due to the underestimation of CMIP5 historical run in these regions.

Region	CMIP5				Regression model			
	DJF	MAM	JJA	SON	DJF	MAM	JJA	SON
N. Africa	-3.8	-3.6	2.4	-16.3	-0.8	-17.7	11.1	-10.3
Middle East	7.8	4.5	6.4	1.5	9.8	-16.0	-5.4	-8.4
N. China	-33.5	-11.4	-9.8	-14.4	312.3	-238.6	-51.2	-30.0
N. America	42.6	26.8	13.2	-6.4	-38.5	-90.0	9.3	-42.4
India	-5.1	0.2	-1.0	-9.9	-27.6	-8.2	-2.9	-32.3
SE. Asia	-45.7	-16.5	-13.5	-17.1	-34.8	1.6	4.2	96.3
S. Africa	24.0	6.1	38.5	54.4	22.3	59.3	231.8	78.3
S. America	35.7	27.4	51.8	36.0	14.8	56.1	78.3	154.6
Australia	-3.2	-3.2	15.3	17.0	2.7	0.4	0.7	3.7

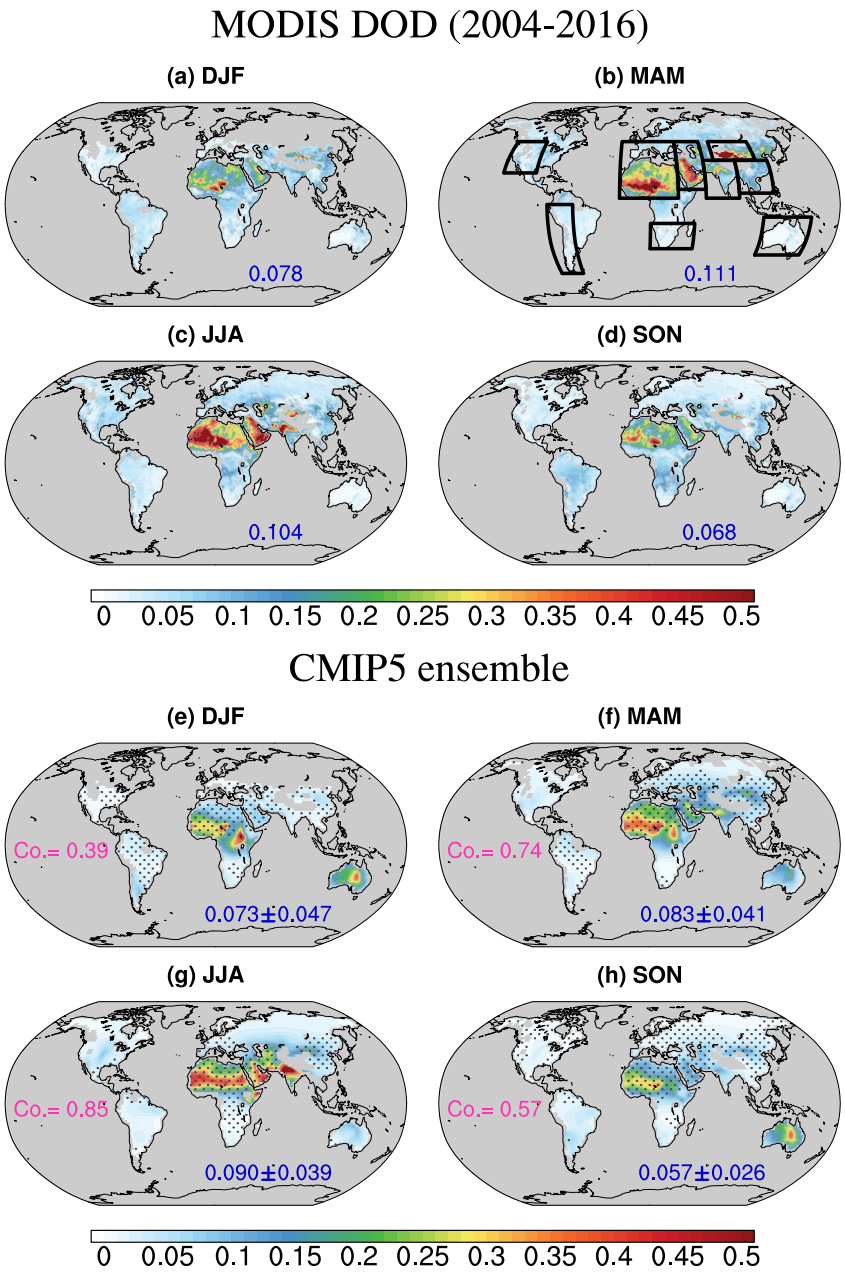

Figure 1. Climatology (2004-2016) of Aqua and Terra combined DOD (i.e., MODIS DOD; top panel) and multi-model mean of CMIP5 DOD (bottom) for four seasons. The pattern correlation (centered; calculated after interpolating MODIS DOD to CMIP5 DOD grids) between CMIP5 and MODIS DOD are shown in pink in the bottom panel. Blue numbers denote global mean DOD over land. For CMIP5 model results, ± one standard deviation among seven CMIP5 models is also shown. Black boxes in (b) denote nine averaging regions (Table 2). Here we only added these boxes in (b) instead of every plot to keep the figure clean. Note that CMIP5 multi-model mean is masked by MODIS DOD for comparison. Dotted area in (e)-(h) shows where multi-model mean is greater than one inter-model standard deviation.

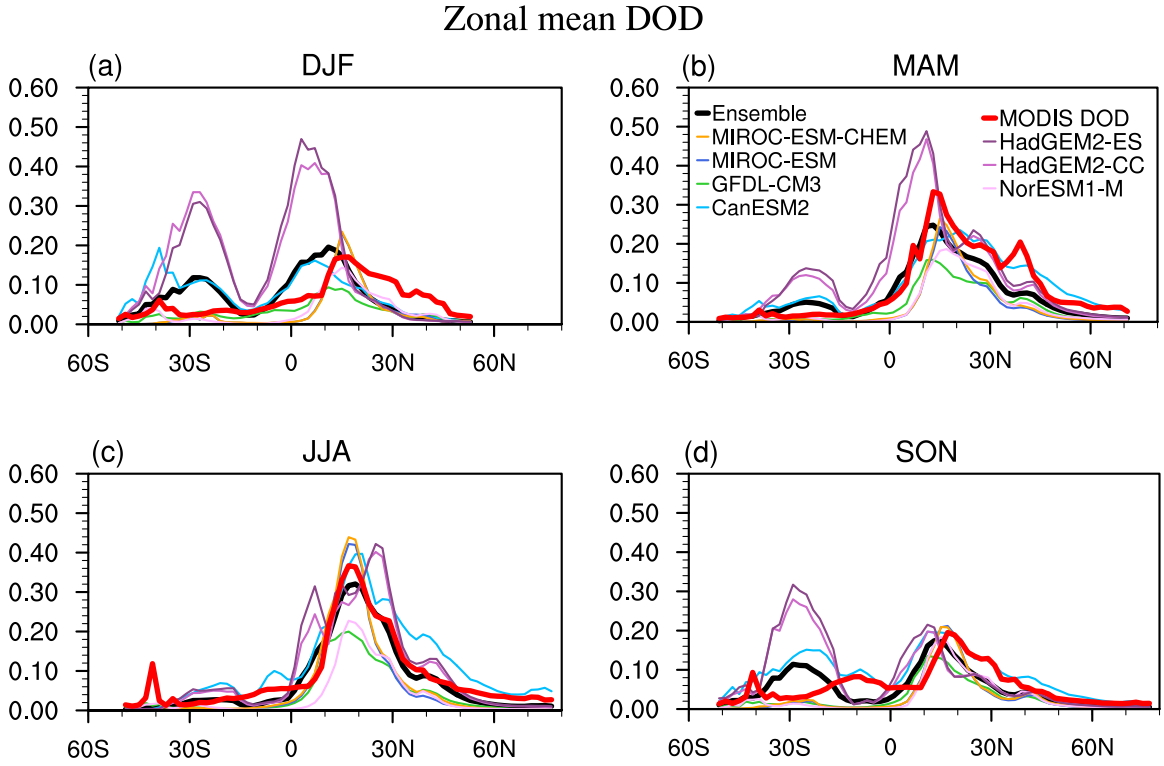

Figure 2. Zonal mean DOD from MODIS (thick red), CMIP5 multi-model mean (thick black), and each individual model (other colorful lines).

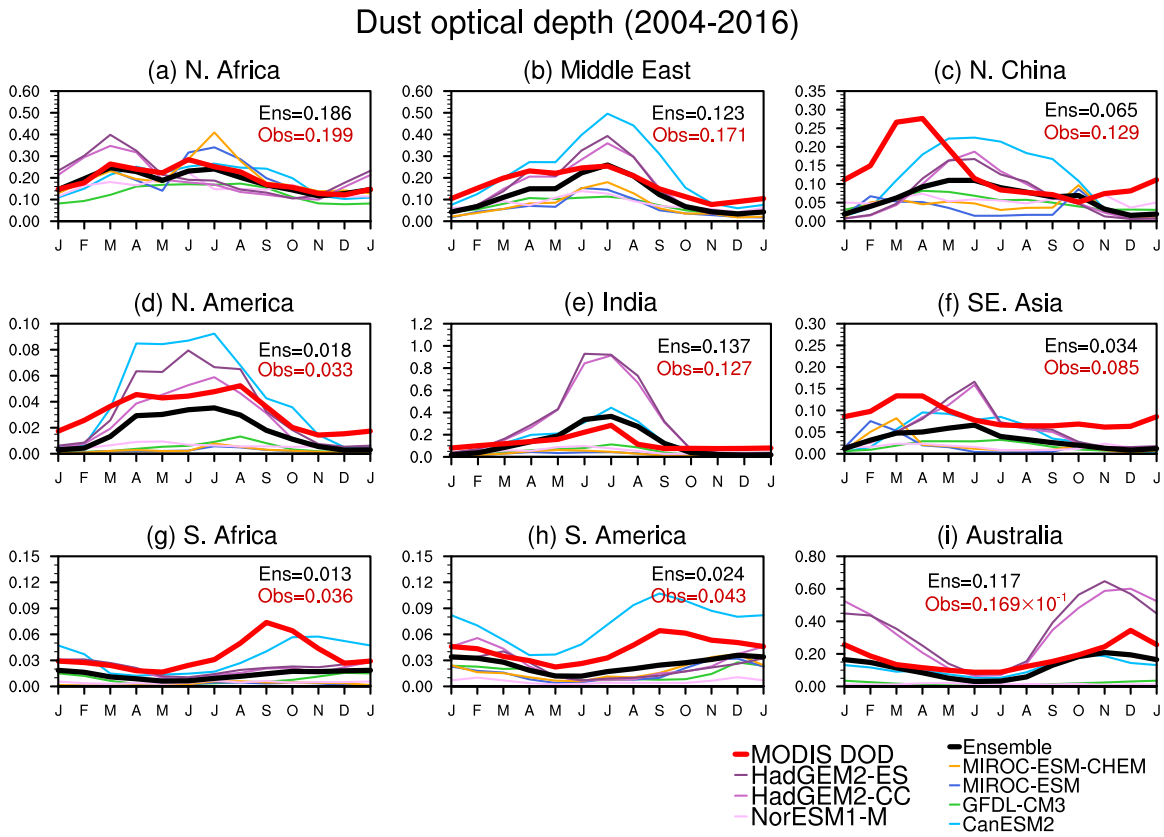

Figure 3. Seasonal cycle of DOD in nine regions (Table 2) averaged over 2004-2016. Thick red lines denote MODIS DOD, thick black lines denote CMIP5 multi-model mean, and other colorful lines denote individual model output. The annual means from MODIS DOD (Obs; red) and multi-model mean (Ens; black) are also listed in each panel. Note that in (i) MODIS DOD (red line) is scaled ten times to better display the season cycle.

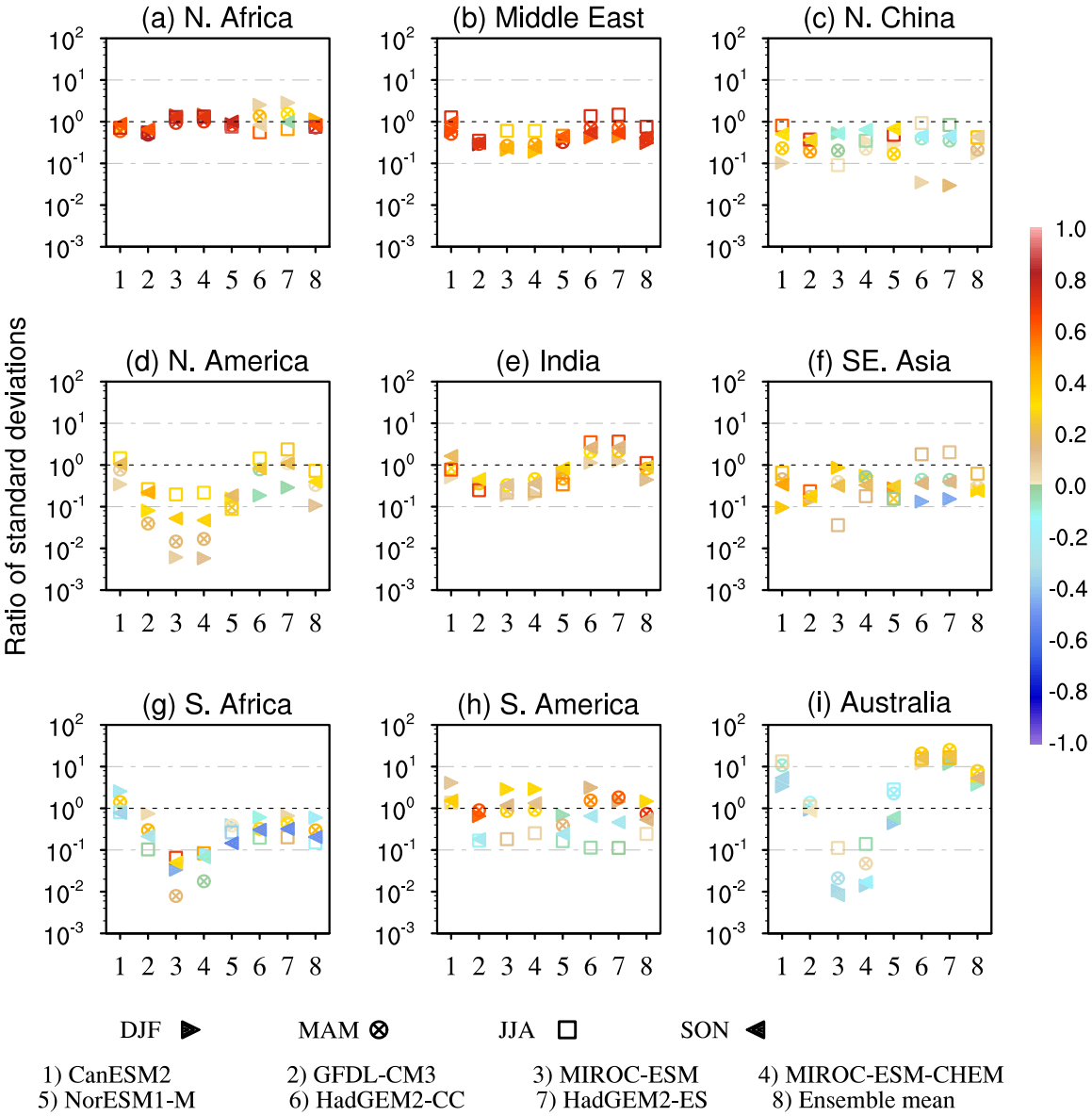

Figure 4. Spatial statistics comparing DOD from CMIP5 models with that from MODIS in nine regions. Label on the X-axis shows individual models (1-7) and multi-model mean (8). Y-axis shows the ratio of pattern standard deviations between model climatology (2004-2016) and that of MODIS, which reveals the relative amplitude of the simulated DOD versus satellite DOD. The color denotes pattern correlation (centered) between each model and MODIS DOD in each region.

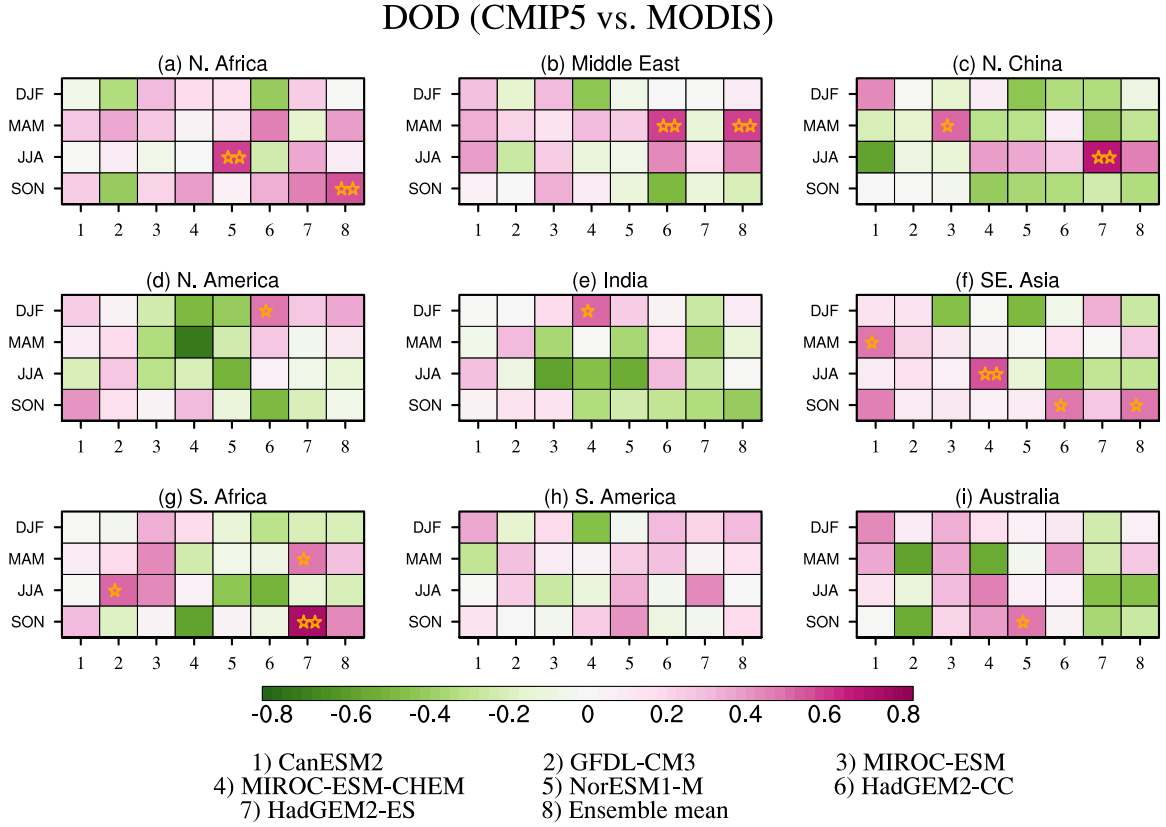

Figure 5. Correlations (color) between regional averaged time series from CMIP5 DOD and MODIS DOD from 2004 to 2016 for four seasons. Numbers in the X-axis denotes each model (1-7) and multi-model mean (8). Correlations significant at the 90% confidence level are marked by a star and significance at the 95% confidence level by two stars.

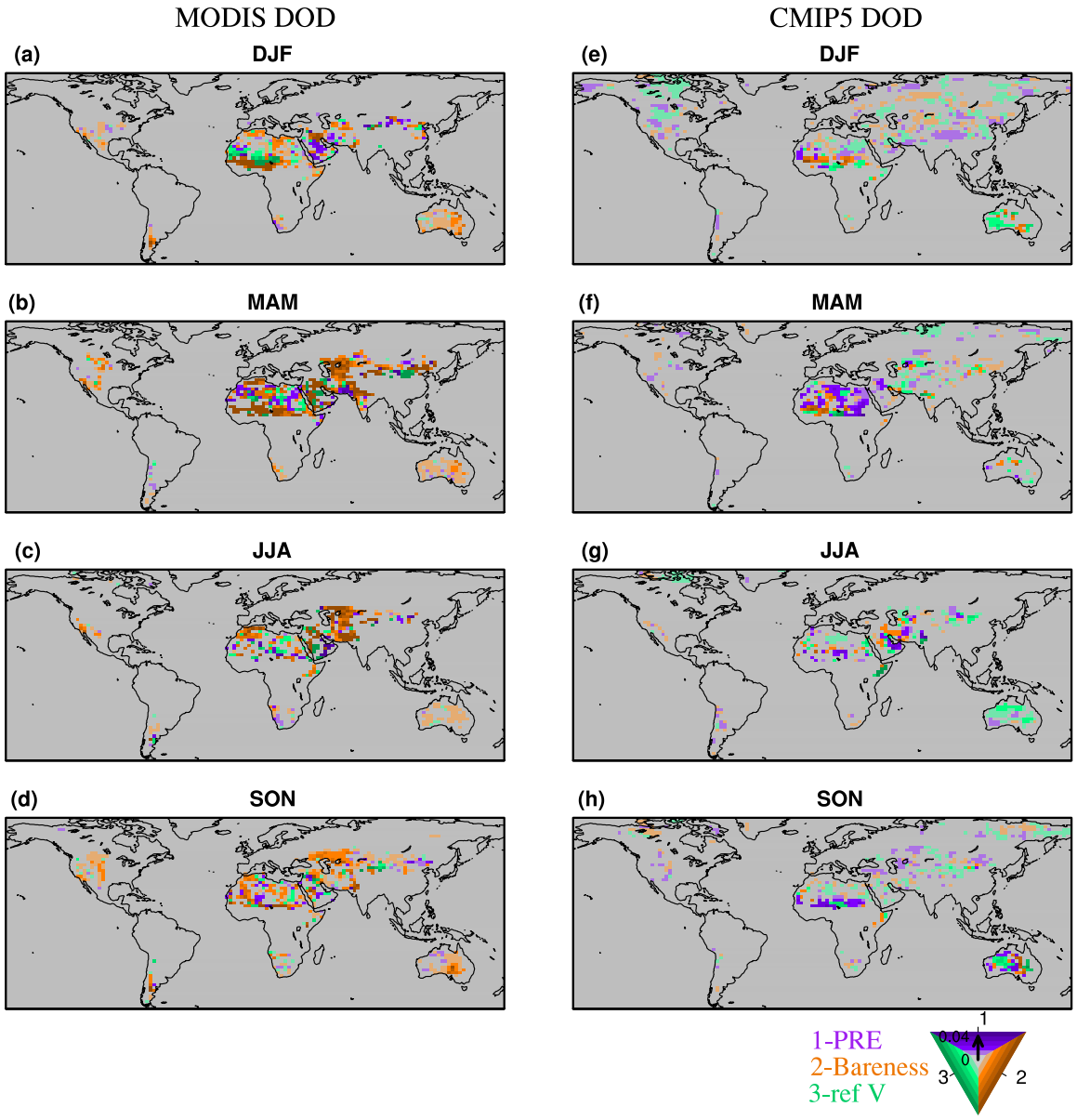

Figure 6. Regression coefficients calculated by regressing DOD in each season onto standardized precipitation (purple), bareness (orange), and surface wind speed (green) from 2004 to 2016. Coefficients obtained using MODIS DOD and observed controlling factors (interpolated to a 2° by 2.5° grid) and those using CMIP5 multi-model mean DOD and controlling factors are shown in the left and right columns, respectively. The color of the shading denotes the largest coefficient in absolute value among the three, while the saturation of the color shows the magnitude of the coefficient (from 0 to 0.04). Only regression coefficients significant at the 90% confidence level (Bootstrap test) are shown. Missing values are shaded in grey. To highlight coefficients near dust source regions, a mask of LAI $\leq$ 0.5 is applied.

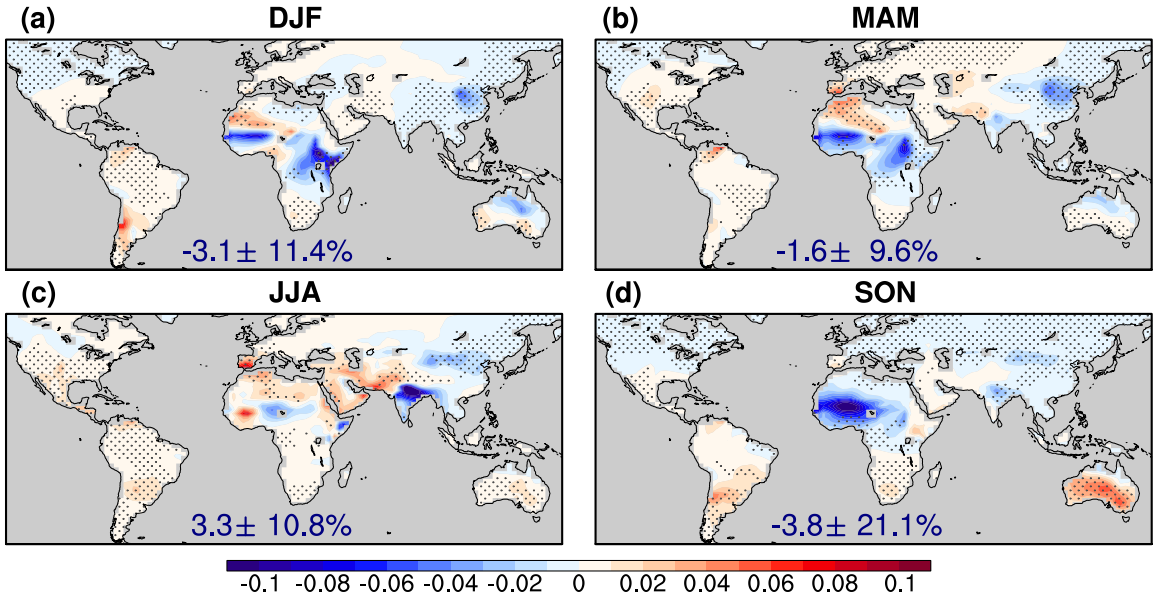

Figure 7. Projected changes of DOD in the late half of the 21st century (under the RCP 8.5 scenario) from that in the historical level (1861-2005) by CMIP5 multi-model mean for four seasons. The percentage change of global mean (over land) DOD ± one inter-model standard deviation is shown at the bottom of each plot. Areas with sign agreement among the models reaches 71.4% (i.e., at least five out of seven models have the same sign as the multi-model mean) are dotted.

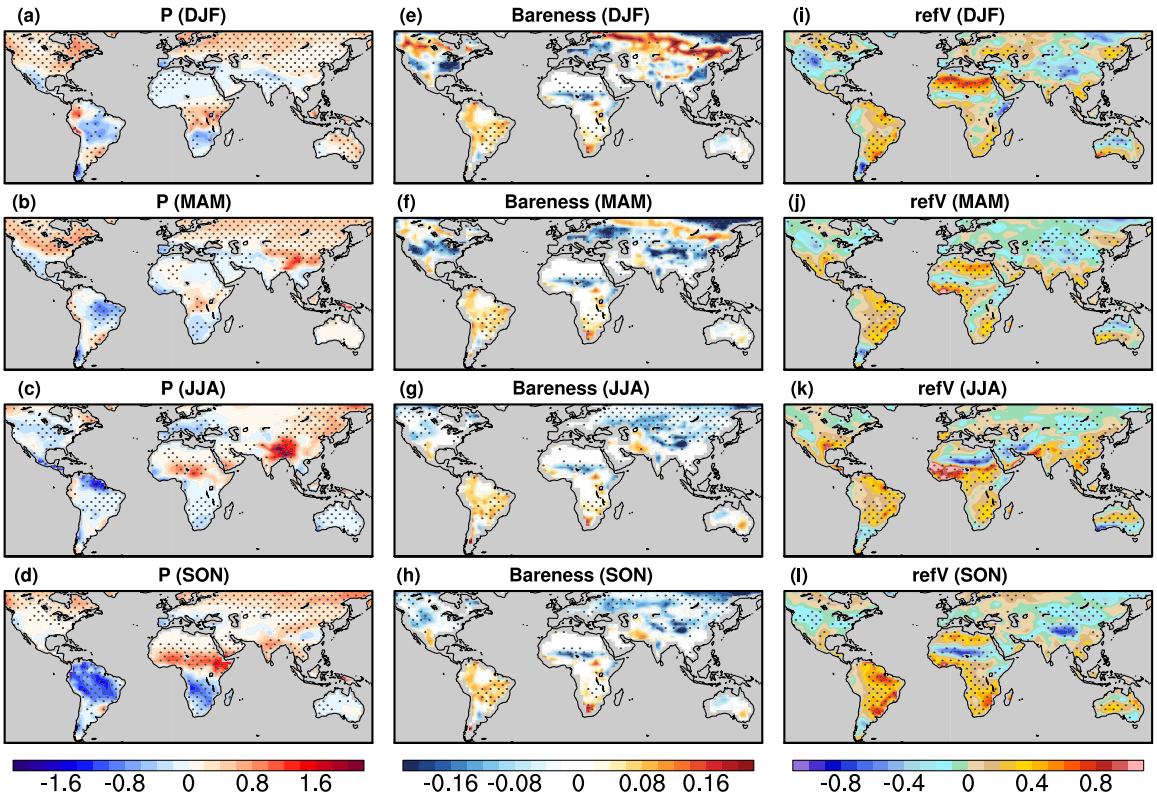

Figure 8. Projected difference of (a)-(d) precipitation (mm day^{-1}), (e)-(h) bareness, and (i)-(l) 10 m wind (m s^{-1}) between the late half of the 21st century (2051-2100; RCP 8.5 scenario) and historical level (1861-2005) from multi-model mean of seven CMIP5 models. Areas with sign agreement among the models reaches 71.4% (i.e., at least five out of seven models have the same sign as the multi-model mean) are dotted.

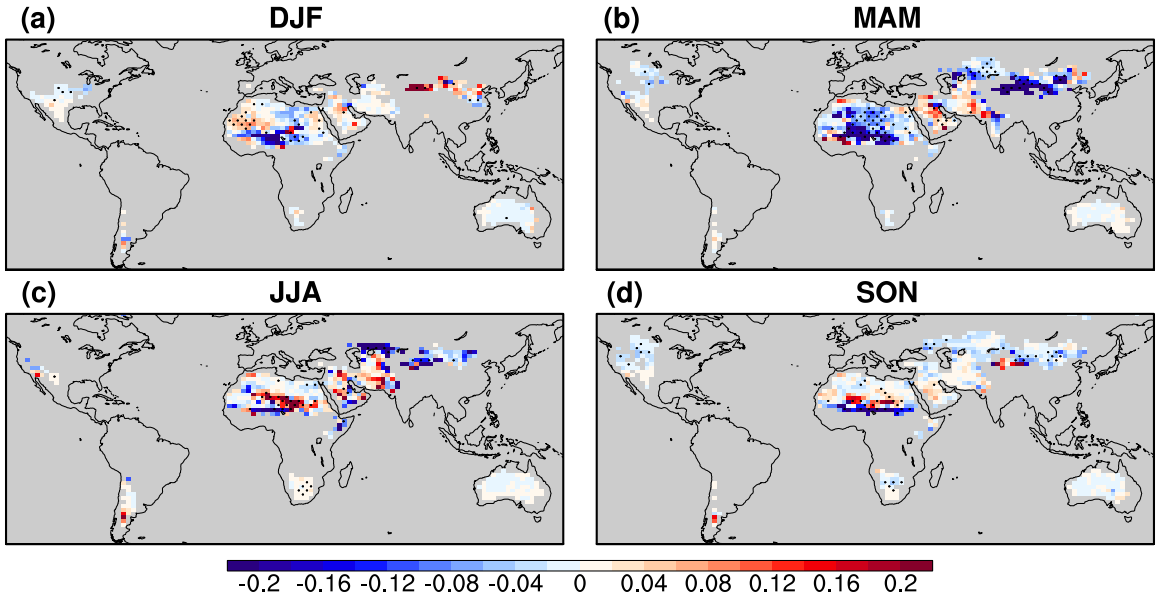

Figure 9. Projected change of DOD in the late half of the 21st century under the RCP 8.5 scenario by the regression model. The results are calculated using the regression coefficients obtained from observations during 2004-2016 (see methodology) and projected changes of precipitation, bareness, and surface wind from seven CMIP5 models. Dotted areas are regions with sign agreement among the regression projections (using output of each of the seven models) above 71.4% (i.e., at least five out of seven regression projections have the same sign as the multi-model mean projection). To highlight DOD variations near the source regions, a mask of LAI $\leq$ 0.5 (from present-day climatology) is applied.

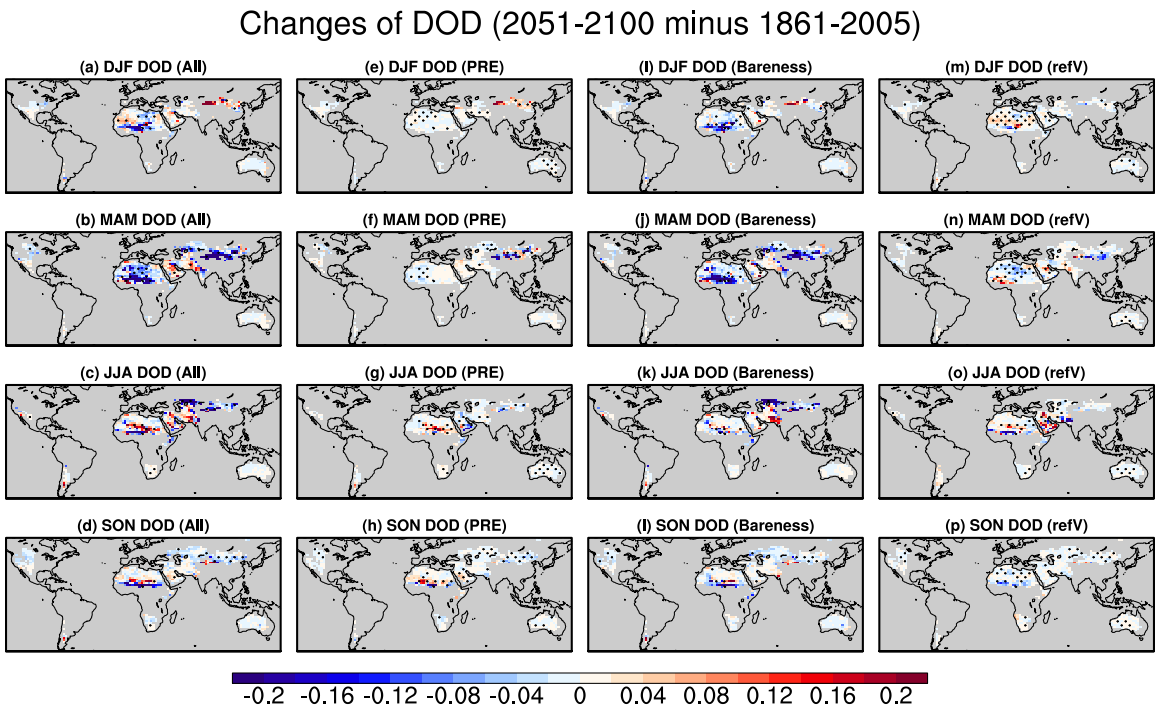

Figure 10. (a)-(d) Projected change of DOD in the late half of the 21st century under the RCP 8.5 scenario by the regression model and output from seven CMIP5 models (same as Fig. 9), and contributions from each component, (e)-(h) precipitation, (j)-(i) bareness, and (m)-(p) surface wind speed. Dotted areas are regions with sign agreement among the projections above 71.4%. To highlight DOD variations near the source regions, a mask of LAI $\leq$ 0.5 (from present-day climatology) is applied.